Spectral Transform Simulations of Turbulent Flows, with Geophysical Applications

D. Ramsden[1], D.Whitfield[1], and G. Holloway[2]

[1]Interact Computing Services
Sidney, B.C. V8L 3S1

[2]Institute of Ocean Sciences
Sidney, B.C. V8L 4B2

Institute of Ocean Sciences
Department of Fisheries and Oceans
Sidney, B.C. V8L 4B2

1985

Canadian Technical Report of Hydrography and Ocean Sciences No. 57

Fisheries and Oceans Pêches et Océans

Canada

Canadian Technical Report of Hydrography and Ocean Sciences

These reports contain scientific and technical information of a type that represents a contribution to existing knowledge but which is not normally found in the primary literature. The subject matter is generally related to programs and interests of the Ocean Science and Surveys (OSS) sector of the Department of Fisheries and Oceans.

Technical Reports may be cited as full publications. The correct citation appears above the abstract of each report. Each report will be abstracted in Aquatic Sciences and Fisheries Abstracts. Reports are also listed in the Department's annual index to scientific and technical publications.

Technical Reports are produced regionally but are numbered and indexed nationally. Requests for individual reports will be fulfilled by the issuing establishment listed on the front cover and title page. Out of stock reports will be supplied for a fee by commercial agents.

Regional and headquarters establishments of Ocean Science and Surveys ceased publication of their various report series as of December 1981. A complete listing of these publications and the last number issued under each title are published in the *Canadian Journal of Fisheries and Aquatic Sciences*, Volume 38: Index to Publications 1981. The current series began with Report Number 1 in January 1982.

Rapport technique canadien sur l'hydrographie et les sciences océaniques

Ces rapports contiennent des renseignements scientifiques et techniques qui constituent une contribution aux connaissances actuelles mais que l'on ne trouve pas normalement dans les revues scientifiques. Le sujet est généralement rattaché aux programmes et intérêts du service des Sciences et Levés océaniques (SLO) du ministère des Pêches et des Océans.

Les rapports techniques peuvent être considérés comme des publications à part entière. Le titre exact figure au-dessus du résumé du chaque rapport. Les résumés des rapports seront publiés dans la revue Résumés des sciences aquatiques et halieutiques et les titres figureront dans l'index annuel des publications scientifiques et techniques du Ministère.

Les rapports techniques sont produits à l'échelon régional mais sont numérotés et placés dans l'index à l'échelon national. Les demandes de rapports seront satisfaites par l'établissement auteur dont le nom figure sur la couverture et la page de titre. Les rapports épuisés seront fournis contre rétribution par des agents commerciaux.

Les établissements des Sciences et Levés océaniques dans les régions et à l'administration centrale ont cessé de publier leurs diverses séries de rapports depuis décembre 1981. Vous trouverez dans l'index des publications du volume 38 du *Journal canadien des sciences halieutiques et aquatiques*, la liste de ces publications ainsi que le dernier numéro paru dans chaque catégorie. La nouvelle série a commencé avec la publication du Rapport n° 1 en janvier 1982.

Canadian Technical Report of Hydrography and Ocean Sciences No. 57

1985

SPECTRAL TRANSFORM SIMULATIONS OF TURBULENT FLOWS, WITH GEOPHYSICAL APPLICATIONS

by

D. Ramsden[1], D. Whitfield[1], and G. Holloway[2]

[1]Interact Computing Services
Sidney, B.C. V8L 3S1

[2]Institute of Ocean Sciences
Sidney, B.C. V8L 4B2

Institute of Ocean Sciences
Department of Fisheries and Oceans
Sidney, B.C. V8L 4B2

Cat. No. Fs97-18/57 ISSN 0711-6764

Correct citation for this publication:

Ramsden, D., D. Whitfield, and G. Holloway. 1985. Spectral Transform Simulations of turbulent flows, with Geophysical Applications. Can. Technical Rep. Hydrogr. and Ocean Sci. 57:54p.

CONTENTS

ABSTRACT

Ramsden, D., D. Whitfield, and G. Holloway. 1985. Spectral Transform Simulations of turbulent flows, with Geophysical Applications. Can. Technical Rep. Hydrogr. and Ocean Sci. 57:54p.

Numerical solutions of barotropic and baroclinic vorticity equations by the method of spectral transforms are presented. Descriptions of the computer simulations, along with criteria for parameterisation of oceanographic and meteorological conditions are given. An analysis of the computational methodology, including aliasing problems and conservation properties is discussed.

Examples are shown for some of the usages of the methods including plume dispersion, plankton patchiness, tracer transport phenomena, predictability or degradation of forecasting, internal wave breaking in a vertical plane, baroclinic instability, eddy/topography interaction and the statistical behaviour of drifter (single point) trajectories.

key words: vorticity, spectral, simulation, plume, plankton, predictability, tracer, dispersion, drifter trajectories.

RÉSUMÉ

Ramsden, D., D. Whitfield, and G. Holloway. 1985. Spectral Transform Simulations of turbulent flows, with Geophysical Applications. Can. Technical Rep. Hydrogr. and Ocean Sci. 57:54p.

Des solutions numériques des équations des tourbillons barotropes et baroclines par la méthode des transformées spectrales sont présentées. Des descriptions des simulations sur ordinateur et des critères de paramétrisation des conditions océanographiques et météorologiques sont données. La méthode de calcul, des problèmes d'aliasing et les propriétés de conservation sont analysés.

On présente des exemples d'application de la méthode à la dispersion des panaches, au caractère épars de plancton, aux phénomènes de transport des marqueurs, à la qualité des prévisions, au déferlement interne des vagues dans un plan vertical, à l'instabilité barocline, à l'interaction entre les tourbillons et le relief et au comportement statistique des trajectoires de dérive d'objets ponctuéls.

Mots cles: tourbillon, spectral, simulation, panache, plancton, prévision, marqueur, dispersion, trajectoires de dérive.

ACKNOWLEDGEMENTS

The authors would like to thank the Ocean Physics Division for their contract support in the development of these programs and for their assistance in providing access to their colour image processor. We want to thank Dorothy Wonnacott for her expert typing, Patricia Kimber for her careful preparation of the figures, and Susan Ball for transcribing some of the equations.

1. INTRODUCTION

This report is a detailed analysis of the development of a set of mathematical techniques and computer programs for the solution of the equations of motion in two dimensions.

In three dimensions, the Navier Stokes equations with the Boussinesq approximations are

$$\frac{\partial}{\partial t}\tilde{u} + 2\Omega \times \tilde{u} + \tilde{u}\cdot\nabla\tilde{u} = -\frac{1}{\rho_0}\nabla p + \frac{g\rho}{\rho_0} + \upsilon\nabla^2\tilde{u} \tag{1.1}$$

$$\nabla\cdot\tilde{u} = 0 \tag{1.2}$$

where $\tilde{u}$ is the velocity field, ρ the density field, ρ_0 the mean density, g the gravity, υ the coefficient of viscosity and $\tilde{u}\cdot\nabla\tilde{u}$ is the dyadic advector operator $(\tilde{u}\cdot\nabla\tilde{u})_i = \sum_j u_j \frac{\partial u_i}{\partial x_j}$. Equation (1.2) is the statement of incompressibility of the fluid under examination.

If we consider oceanic motion on time scales rather longer than a day, then the strong constraint due to the earth's rotation permits a further simplification. We may omit dependence upon the local vertical coordinate, thus resolving only the two horizontal coordinates. This approximation will tend to be valid if we consider only horizontal length scales larger than the first internal Rossby radius of deformation or, typically, twenty times the depth of the water column at mid-latitude. At higher latitudes, given weak stratification and strong rotation, smaller horizontal scales of motion down to just a few times the depth of water may be considered as two-dimensional. $\tilde{u}$ can then be approximated by $\tilde{u}_H$, in which w, the vertical velocity, is zero. It is now possible to rewrite equation (1.1) in terms of a stream function ψ with $\tilde{u}$ being defined by

$$\tilde{u} = \hat{k} \times \nabla\psi \tag{1.3a}$$

Let

$$\xi \equiv \nabla \times \tilde{u} = \nabla^2\psi \tag{1.3b}$$

When these equations (1.3a) and (1.3b) are introduced into equation (1.1), we get the equations of barotropic vorticity conservation.

$$\frac{\partial}{\partial t}\xi + J(\psi,\xi) = \nu^2\xi \tag{1.4}$$

$$\text{with } J(A,B) \equiv \frac{\partial A}{\partial x}\frac{\partial B}{\partial y} - \frac{\partial A}{\partial y}\frac{\partial B}{\partial x} \tag{1.5}$$

This equation of two dimensional geostrophic turbulence is complicated somewhat when we add such things as planetary vorticity and topographic interaction due to vortex stretching and mean flow. This will be discussed in detail in Section 4.

Equation (1.4) will be modified for forcing and a gravity potential energy term. When multiple layers are considered, there will be coupling terms amongst the layers.

The solution of (1.4) and its derivative equations give us a rich set of problems to address. The expression in the spectral domain allows flexibility in choosing initial conditions and forcing conditions. There is also the flexibility to deal with physical effects in either the real or spectral domain. Spectra of kinetic energy ($\equiv k^2|\psi|^2$) can be prescribed (k a wave number), real topographic ridges, isolated pieces of topography, and/or a spectrum of topography can be specified. Floats can be dropped into regions of interest and the response of passive tracers to the flow field can be measured. The model can be turned on end using an x-z plane to model internal waves in 2 dimensions. Runs can be duplicated to test the effects of various parameters such as β, or different types of diffusion. Mean flow shear, or a series of shears, can be prescribed and systematic responses can be examined. The model can be reached into at any point, and a wealth of statistical quantities to accurately test theoretical results can be developed.

The major limitation of the method is that, because we deal with the equations in the Fourier domain, the boundary conditions must be periodic. This presents difficulties in modelling basins, for example.

2. SPECTRAL TRANSFORM METHOD

2.0 Overview

The purpose of this section is to describe a numerical method, due to Orszag (1971), which may be used to solve equations for the advection and diffusion of vorticity, heat or dissolved substances in fluids subject to periodic boundary conditions.

Orszag's method starts by Fourier transforming the partial differential equations of motion to a finite grid in spectral space, where they become coupled first-order ordinary differential equations. The non-linear advection terms which require a prohibitive amount of computation in spectral space are evaluated by transforming the necessary fields to physical space, taking local products and transforming the results to spectral space. Special procedures are used to eliminate aliasing. When fast Fourier transforms (FFT's) are employed for this process, the Orszag spectral method becomes computationally competitive with finite difference methods and may provide for high resolution in two, and, especially, three dimensions.

There are advantages of this method beyond computational efficiency:

i) for a given number of grid points, accuracy is likely to be greatly improved, as derivatives are represented effectively to infinite order. A corollary of this is that phase relationships are preserved. Computational wave phase speeds are equal to theoretical speeds. No distortion of group velocity occurs and hence energy and momenta transfers are treated correctly.

ii) Energy, enstrophy, variance of tracer field and various correlations are semi-conserved (i.e. conserved aside from time-differencing errors and viscous or diffusive dissipation).

2.1 Transformation to spectral space

As a particular example, easily generalized, we treat the viscid vorticity equation in two dimensions

$$\frac{\partial}{\partial t}\nabla^2\psi + J(\psi,\nabla^2\psi) - \nu\nabla^4\psi = 0 \tag{2.1.1}$$

ψ being a stream function representing the velocity field, ν viscosity, and the Jacobian determinant is

$$J(\psi,\nabla^2\psi) = \frac{\partial\psi}{\partial x}\frac{\partial\nabla^2}{\partial y}\psi - \frac{\partial\psi}{\partial y}\frac{\partial}{\partial x}\nabla^2\psi \tag{2.1.2}$$

The periodic boundary condition is

$$\psi(x+X,y+Y,t) = \psi(x,y,t) \tag{2.1.3}$$

Define spatial grid by

$$\begin{aligned} X_\alpha &= \frac{\alpha X}{Nx} \quad , \ \alpha = 0,1,2,\ldots.Nx-1 \\ Y_\beta &= \frac{\beta Y}{Ny} \quad , \ \beta = 0,1,\ldots\ldots Ny-1 \end{aligned} \tag{2.1.4}$$

then ψ is approximated by a Fourier series

$$\psi(x_\alpha,y_\beta,t) = \psi_{\alpha\beta}(t) = \sum_{m=-\frac{Nx}{2}}^{\frac{Nx}{2}-1}\ \sum_{n=-\frac{Ny}{2}}^{\frac{Ny}{2}-1} \psi_{mn(t)}\ \exp\{i(k_m x_\alpha + \ell_n y_\beta)\} \tag{2.1.5}$$

where the wavenumbers take the values

$$k_m = \frac{2\Pi m}{X} \quad , \quad \ell_n = \frac{2\Pi n}{Y} \tag{2.1.6}$$

therefore,

$$\psi_{\alpha\beta}(t) = \sum_{m=-\frac{Nx}{2}}^{\frac{Nx}{2}-1}\ \sum_{n=-\frac{Ny}{2}}^{\frac{Ny}{2}-1} \psi_{mn}(t).\ \exp\{i2\Pi(\frac{m\alpha}{Nx} + \frac{n\beta}{Ny})\} \tag{2.1.7}$$

the inverse of this transform is

$$\psi_{mn} = \frac{1}{NxNy}\sum_{\alpha=0}^{Nx-1}\ \sum_{\beta=0}^{Ny-1} \psi_{\alpha\beta}\ \exp\{-i2\Pi(\frac{m\alpha}{Nx} + \frac{n\beta}{Ny})\} \tag{2.1.8}$$

Because $\psi(x,y,t)$ is real, ψ_{mn} is conjugate symmetric

$$\psi_{mn} = \psi^*_{-m,-n} \qquad (2.1.9)$$

where the superscript asterisk denotes complex conjugation.

The spatial derivative terms in (2.1.1) take a very simple form;

$$\nabla^2\psi(X_\alpha,Y_\beta,t) = \sum_m \sum_n -(k_m^2+\ell_n^2)\cdot\psi_{mn}(t).\exp\{i(k_mX_\alpha+\ell_nY_\beta)\} \qquad (2.1.10)$$

$$\nabla^4\psi(X_\alpha,Y_\beta,t) = \sum_m \sum_n +(k_m^2+\ell_n^2)^2\cdot\psi_{mn}(t).\exp\{i(k_mX_\alpha+\ell_nY_\beta)\} \qquad (2.1.11)$$

Defining J_{mn} by

$$J(\psi,\nabla^2\psi) = \sum_m \sum_n J_{mn}\exp\{i(k_mx_\alpha+\ell_nY_\beta)\} \qquad (2.1.12)$$

substitution into (2.1.1) yields

$$\frac{d\psi_{mn}}{dt} = \frac{J_{mn}}{k_m^2+\ell_n^2} - \nu(k_m^2+\ell_n^2)\psi_{mn} \qquad (2.1.13)$$

The original partial differential equation has been replaced by a set of coupled first order ordinary DE's, the numerical solution of which is straightforward (Section 2.3), provided that a suitable procedure is available for evaluating the J_{mn}'s. Explanation of such a procedure constitutes much of the remaining theoretical part of this report.

2.2 Evaluation of the advective term

The material of this section is very technical, and a first-time reader may find it useful to skip to Section 2.3 and return to this section with a better overview of the whole spectral transform method.

Correct calculation of the J_{mn}'s defined by (2.1.9), is a complex process, and it is only the availability of FFT algorithms which makes Orszag's spectral method computationally advantageous.

For the remainder of this section we will follow Davey (1980) fairly closely.

2.2.1 Derivation of formulae

The derivation is simplified if the Jacobian is first expressed in a particular form. Fluid velocity components are derived from the stream function, ψ:

$$u_x = -\frac{\partial \psi}{\partial y} \quad , \quad u_y = \frac{\partial \psi}{\partial x} \tag{2.2.1}$$

Let

$$\chi = \nabla^2 \psi \tag{2.2.2}$$

Then

$$\begin{aligned} J(\psi, \nabla^2\psi) &= \underline{u} \cdot \nabla \chi \\ &= \nabla \cdot (\underline{u}\chi) \\ &= \frac{\partial}{\partial x}(u_x \chi) + \frac{\partial}{\partial y}(u_y \chi) \end{aligned} \tag{2.2.3}$$

Now (2.1.4), with a change of subscript symbols, and the corresponding Fourier series expansion of χ are

$$\psi(x,y,t) = \sum_p \sum_q \psi_{pq} \cdot e^{i(K_p x_\alpha + \ell_q y_\beta)} \tag{2.2.4}$$

$$\chi(x,y,t) = \sum_r \sum_s \chi_{rs} \cdot e^{i(K_r x_\alpha \ell_s y_\beta)} \tag{2.2.5}$$

Then the first term on the RHS of (2.2.3) is

$$\frac{\partial}{\partial x}\left(\frac{-\partial \psi}{\partial y}\chi\right) = \frac{\partial}{\partial x}\left[\sum_p \sum_q i\ell_q \cdot \psi_{pq} \cdot e^{i(K_p x_\alpha + \ell_q y_\beta)} \sum_r \sum_s \chi_{rs} \cdot e^{i(K_r x_\alpha + \ell_s y_\beta)}\right]$$

$$= \sum_p \sum_q \sum_r \sum_s -\ell_q (K_p + K_r) \cdot \psi_{pq} \cdot \chi_{rs}\, e^{i(K_p + K_r)\chi_\alpha} \cdot e^{i(\ell_q + \ell_s) y_\beta}$$

Let

$$u_{pq} = -i\ell_q \psi_{pq}$$

Then

$$\frac{\partial}{\partial x}\left(\frac{-\partial \psi}{\partial y} \cdot \chi\right) = \sum_p \sum_q \sum_r \sum_s i(K_p + K_r)\, U_{pq} \chi_{rs}\, e^{i(K_p + K_r)x} \cdot e^{i(\ell_q + \ell_s)y}$$

and, with the definition

$$V_{pq} = i_p \psi_{pq}$$

$$\frac{\partial}{\partial y}\left(\frac{\partial \psi}{\partial x} \cdot \chi\right) = \sum_p \sum_q \sum_r \sum_s i(\ell_q + \ell_s) \cdot V_{pq} \cdot \chi_{rs}\, e^{i(K_p + K_r)x} \cdot e^{i(\ell_q + \ell_s)y}$$

Thus,

$$J(\psi,\nabla^2\psi) = \sum_{pprs}\sum\sum\sum i\,(k_p+k_r)u_{pq}+(\ell_q+\ell_s)v_{pq}\,\chi_{rs}\,\exp\{i(k_p+k_r)x\,\exp\{i(\ell_q+\ell_s)y\} \quad (2.2.6)$$

Comparing (2.2.6) and (2.1.9), we see that their equivalence requires

$$J_{mn}=\sum_p\sum_q\sum_r\sum_s\left[i(K_p+K_r)U_{pq}+i(\ell_q+\ell_s)V_{pq}\right]\chi_{rs}\,\delta(p+r-m)\delta(q+s-n)$$

$$=iK_m\sum_p\sum_q\sum_r\sum_s\left[U_{pq}\cdot\chi_{rs}\cdot\delta(p+r-m)\delta(q+s-n)\right] \quad (2.2.7)$$

$$+i\ell_n\sum_p\sum_q\sum_r\sum_s\left[V_{pq}\cdot\chi_{rs}\cdot\delta(p+r-m)\delta(q+s-n)\right]$$

If this was the final formula for J_{mn} the spectral method could be very inefficient, as $\mathcal{O}(N_x N_y)$ arithmetic operations are required for its evaluation. Orszag's contribution was to find a procedure to greatly reduce the computational load.

Let

$$W_{mn}=\sum_p\sum_q\sum_r\sum_s U_{pq}\chi_{rs}\,\delta(p+r-m)\delta(q+s-n) \quad (2.2.8)$$

Transform u to a physical space grid.

$$\hat{U}_{\alpha,\beta}=\sum_{p=-\frac{N_x}{2}}^{\frac{N_x-1}{2}}\sum_{q=-\frac{N_y}{2}}^{\frac{N_y-1}{2}}U_{pq}\,e^{i2\pi\left(\frac{p\alpha}{N_x}+\frac{q\beta}{N_y}\right)} \quad (2.2.9)$$

and similarly for $\hat{\chi}_{\alpha,\beta}$

Then form the local product, $\hat{U}_{\alpha\beta}\hat{\chi}_{\alpha\beta}$, at each grid point in physical space and transform it to spectral space.

$$\hat{W}_{mn}=\frac{1}{N_xN_y}\sum_{\alpha=0}^{N_x-1}\sum_{\beta=0}^{N_y-1}\hat{U}_{\alpha\beta}\hat{\chi}_{\alpha\beta}\,e^{-i2\pi\left(\frac{m\alpha}{N_x}+\frac{n\beta}{N_y}\right)}$$

$$=\frac{1}{N_xN_y}\sum_\alpha\sum_\beta\left[\sum_p\sum_q U_{pq}\cdot e^{i2\pi\left(\frac{p\alpha}{N_x}+\frac{q\beta}{N_y}\right)}\right]\left[\left(\sum_r\sum_s\chi_{rs}e^{i2\pi\left(\frac{r\alpha}{N_x}+\frac{s\beta}{N_y}\right)}\right]e^{-i2\pi\left(\frac{m\alpha}{N_x}+\frac{n\beta}{N_y}\right)}\right.$$

$$=\sum_p\sum_q\sum_r\sum_s U_{pq}\cdot\chi_{rs}\left[\frac{1}{N_xN_y}\sum_\alpha\sum_\beta e^{i2\pi\left(\frac{p\alpha}{N_x}+\frac{q\beta}{N_y}+\frac{r\alpha}{N_x}+\frac{s\beta}{N_y}-\frac{m\alpha}{N_x}-\frac{n\beta}{N_y}\right)}\right]$$

We invoke the appropriate orthogonality theorem:

$$\sum_{\alpha=0}^{N-1}e^{\frac{i2\pi}{N}(p+r-m)\alpha} \qquad = N,\ p+r-m=0,\ \pm N,\pm 2N\ \ldots.$$

$$= 0 \quad \text{otherwise}$$

therefore

$$\hat{W}_{mn} = \sum_p \sum_q \sum_r \sum_s U_{pq} \chi_{rs} \cdot \delta(p+r-m-jN_x) \cdot \delta(q+s-n-\ell N_y) \tag{2.2.10}$$

with $j, \ell = 0, \pm 1$. Because wavenumbers are bound by $\pm K$, larger j, ℓ will not occur.

We separate and give symbols to the terms of (2.2.10):

$$\hat{W}_{mn} = W_{mn} + W(m, n \pm N_y) + W(m \pm N_x, N) + W(m \pm N_x, n \pm N_y) \tag{2.2.11}$$

The first term is that which we seek; the remaining three are the contributions of aliasing, which is the artificial introduction of high wave number components inherent in finite Fourier transforms. Following Orszag, we perform a new set of transforms on a spatial grid which is shifted w.r.t. the previous one by one-half grid interval in both directions:

$$\begin{aligned} \tilde{U}_{\alpha\beta} &= \sum_p \sum_q U_{pq} e^{i2\pi \left[\frac{p(\alpha+1/2)}{N_x} + \frac{q(\beta+1/2)}{N_y} \right]} \\ &= \sum_p \sum_q U_{pq} e^{i2\pi \left(\frac{p\alpha}{N_x} + \frac{q\beta}{N_y} \right)} \cdot e^{i\pi \left(\frac{p}{N_x} + \frac{q}{N_y} \right)} \end{aligned} \tag{2.2.12}$$

and similarly for $\tilde{\chi}_{\alpha\beta}$. Then proceeding as above,

$$\begin{aligned} \tilde{W}_{mn} &= \frac{1}{N_x N_y} \sum_\alpha \sum_\beta \tilde{U}_{\alpha\beta} \tilde{\chi}_{\alpha\beta} e^{-i2\pi \left[\frac{m}{N_x}(\alpha+\frac{1}{2}) + \frac{n}{N_y}(\beta+\frac{1}{2}) \right]} \\ &= \frac{1}{N_x N_y} \sum_\alpha \sum_\beta \left[\left\{ \sum_p \sum_q U_{pq} e^{i2\pi \left(\frac{p\alpha}{N_x} + \frac{q\beta}{N_y} \right)} \cdot e^{i\pi \left(\frac{p}{N_x} + \frac{q}{N_y} \right)} \right\} \left\{ \sum_r \sum_s \chi_{rs} \cdot e^{i2\pi \left(\frac{r\alpha}{N_x} + \frac{s\beta}{N_y} \right)} \right. \right. \\ &\quad \left. \left. \cdot e^{i\pi \left(\frac{r}{N_x} + \frac{s}{N_y} \right)} \cdot e^{-i2\pi \left(\frac{m\alpha}{N_x} + \frac{n\beta}{N_y} \right)} e^{-i\pi \left(\frac{m}{N_x} + \frac{n}{N_y} \right)} \right\} \right] \\ &= \sum_p \sum_q \sum_r \sum_s U_{pq} \chi_{rs} e^{i\pi \left(\frac{p+r-m}{N_x} + \frac{q+s-n}{N_y} \right)} \cdot \delta(p+r-m-jN_x) \cdot \delta(q+s-n-\ell N_y) \\ &= \sum_p \sum_q \sum_r \sum_s U_{pq} \chi_{rs} e^{i\pi \left(\frac{jN_x}{N_x} + \frac{\ell N_y}{N_y} \right)} \cdot \delta(p+r-m-jN_x) \cdot \delta(q+s-n-\ell N_y) \\ &= \sum_p \sum_q \sum_r \sum_s U_{pq} \chi_{rs} (-)^{j+\ell} \cdot \delta(p+r-m-jN_x) \cdot \delta(q+s-n-\ell N_y) \end{aligned} \tag{2.2.13}$$

$$\tilde{W}_{mn} = W_{mn} - W(m, \pm N_y) - W(m \pm N_x, n) + W(m \pm N_x, n \pm N_y) \tag{2.2.14}$$

Thus

$$\tfrac{1}{2}(W_{mn} + W_{mn}) = W_{mn} + W(m \pm N_x, n \pm N_y) \qquad (2.2.15)$$

which contains only one unwanted term. This term may be eliminated by setting all spectral components to zero outside of a suitable domain. For the case of $N_x = N_y = N$, this domain may be circular (Patterson and Orszag, 1971)

$$p^2 + q^2 < \frac{8}{9}\left(\frac{N}{2}\right)^2 \quad , \quad r^2 + s^2 < \frac{8}{9}\left(\frac{N}{2}\right)^2 \qquad (2.2.16)$$

or octagonal (Orszag, 1971)

$$|p| < \frac{N}{2} \ , \ |q| < \frac{N}{2} \ , \ |p + q| < \frac{4}{3}\ \frac{N}{2} \qquad (2.2.17)$$

when $N_x = N_y$, (2.2.16) is easily generalized to an elliptical domain

$$\left(\frac{2p}{N_x}\right)^2 + \left(\frac{2q}{N_y}\right)^2 < \frac{8}{9} \quad , \quad \left(\frac{2r}{N_x}\right)^2 + \left(\frac{2s}{N_y}\right)^2 < \frac{8}{9} \qquad (2.2.18)$$

The octagonal domain contains more modes than the circular, but introduces an anisotrophy which may be undesirable. Proofs of these results are available in the original papers. Further, Patterson and Orszag (1971) show that (2.2.16) represents the worst case limitation for circular domains and give formulae for larger domain radii as functions of $\frac{N}{2}$.

At this point, we have a completely de-aliased algorithm for the computation of J_{mn}. Before proceeding to show how standard FFT routines may be utilized, a summary may be clarifying;

$$U_{pq} = -i l_q \psi_{pq}$$

$$V_{pq} = i K_p \psi_{pq}$$

$$\chi_{rs} = -(K_r^2 + l_s^2)\psi_{rs}$$

$$\hat{U}_{\alpha\beta} = \sum_{p=-\frac{N_x}{2}}^{\frac{N_x}{2}-1} \sum_{q=-\frac{N_y}{2}}^{\frac{N_y}{2}-1} U_{pq}\, e^{i2\pi\left(\frac{p\alpha}{N_x} + \frac{q\beta}{N_y}\right)}$$

$$\hat{\chi}_{\alpha\beta} = \sum_r \sum_s \chi_{rs}\, e^{i2\pi\left(\frac{r\alpha}{N_x} + \frac{s\beta}{N_y}\right)}$$

$$\tilde{U}_{\alpha\beta} = \sum_p \sum_q \left[U_{pq} e^{i\pi\left(\frac{p}{N_x} + \frac{q}{N_y}\right)} \right] \cdot \left[e^{i2\pi\left(\frac{p\alpha}{N_x} + \frac{q\beta}{N_y}\right)} \right]$$

$$\tilde{\chi}_{\alpha\beta} = \sum_r \sum_s \left[\chi_{rs} e^{i\pi\left(\frac{r}{N_x} + \frac{s}{N_y}\right)} \right] \cdot \left[e^{i2\pi\left(\frac{r\alpha}{N_x} + \frac{s\beta}{N_y}\right)} \right]$$

$$\hat{W}_{mn} = \frac{1}{N_x N_y} \sum_{\alpha=0}^{N_x-1} \sum_{\beta=0}^{N_y-1} \hat{U}_{\alpha\beta} \cdot \hat{\chi}_{\alpha\beta} \cdot e^{i2\pi\left(\frac{m\alpha}{N_x} + \frac{n\beta}{N_y}\right)}$$

$$\tilde{W}_{mn} = \frac{1}{N_x N_y} \left[\sum_\alpha \sum_\beta \tilde{U}_{\alpha\beta} \tilde{\chi}_{\alpha\beta} e^{-i2\pi\left(\frac{m\alpha}{N_x} + \frac{n\beta}{N_y}\right)} \right] \cdot e^{-i\pi\left(\frac{m}{N_x} + \frac{n}{N_y}\right)}$$

$$W_{mn} = \frac{1}{2} \left[\hat{W}_{mn} + \tilde{W}_{mn} \right]$$

Similarly for V_{mn}. Finally

$$J_{mn} = iK_m W_{mn} + il_n V_{mn}$$

A total of ten transforms is required ($\hat{\chi}_{\alpha\beta}$ and $\tilde{\chi}_{\alpha\beta}$ are saved and used twice).

2.2.2 Using standard FFT routines

Most standard, packaged, FFT routines perform the transform pair

$$f_{m'} = \frac{1}{N} \sum_{p=0}^{N-1} F_p e^{-\frac{i2\pi m' p}{N}} \qquad 0 < m' < N$$

$$F_p = \sum_{m'=0}^{N-1} f_{m'} e^{\frac{i2\pi m' p}{N}} \qquad 0 < p < N$$

How do we use these to achieve the transforms we require?

Consider the forward transform first. We want $\frac{-N}{2} \leq m < \frac{N}{2}$ forward.

Since $$f_m = \frac{1}{N} \sum_{p=0}^{N-1} F_p e^{\frac{-i2\pi m p}{N}}$$

$$e^{\frac{-i2\pi(m'-N)p}{N}} = e^{\frac{-i2\pi m' p}{N}} \cdot e^{i2\pi p} = e^{\frac{-i2\pi m' p}{N}}$$

then the correspondence between m' and m is as follows:

m'	$0, 1, 2 \ldots, \frac{N}{2}-1, \frac{N}{2}, \frac{N}{2}+1, \ldots, N-1$
m	$0, 1, 2 \ldots, \frac{N}{2}-1, \frac{-N}{2}, \frac{-N}{2}+1, \ldots, -1$

Therefore, the package routine does what we want, but leaves the spectral coefficients in this special order. If the package inverse transform is now applied to a field of spectral coefficients which are stored in this order:

$$F_p = \sum_{m=0}^{\frac{N}{2}-1} f_m e^{\frac{i2\pi m p}{N}} + \frac{1}{N} \sum_{m=-\frac{N}{2}}^{-1} f_m e^{\frac{i2\pi p (m+N)}{N}}$$

$$= \frac{1}{N} \sum_{m=-\frac{N}{2}}^{\frac{N}{2}-1} f_m e^{\frac{i2\pi m p}{N}}$$

This is what is wanted.

To make use of these results in simulation, the two (or three) dimensional spectral field is stored in an order derived from that given above. The wavenumber array, k_m and ℓ_n, is stored in the same order. In Table 1 this order is illustrated: for the case of the Floating Point Systems two-dimensional real-to-complex transforms.

Once the correct values and order of storage for k_m, ℓ_m and combinations of them are determined, any desired derivative is performed in spectral space by an array multiplication (and subsequent real or imaginary swaps and negations to represent multiplication by $\sqrt{-1}$, if required).

Table 1. The FPS 190L K space map for a 2d FFT.

K space N x N array m = N/2
(Ky, Kx) representation

J \ I	1	2	3	4	5		n-1	n
1	r(0,0)	r(0,m)	r(0,1)	i(0,1)	r(0,2)	....	r(0,m-1)	i(0,m-1)
2	r(m,0)	r(m,m)	r(1,1)	i(1,1)	r(1,2)	....	r(1,m-1)	i(1,m-1)
3	r(1,0)	r(1,m)	r(2,1)	i(2,1)	"	....	"	
4	i(1,0)	i(1,m)	r(3,1)	"	"	....	"	
5	r(2,0)	r(2,m)	r(4,1)	"	"	....	"	
'	"	"	"	"	"	....	"	
'	"	"	"	"	"	....	"	
'	"	"	"	"	"	....	"	
n/2	i(m/2,0)	i(m/2,m)	r(m,1)	i(m,1)	r(m,2)	....	r(m,m-1)	i(m,m-1)
n/2+1	r(m/2+1,0)	r(m/2+1,0)	r(m+1,1)	i(m+1,1)	r(m+1, 2)	....	r(-m+1, m-1)	i(-m+1, m-1)
'	"		"	"	"	....		
'	"		"	"	"	....		
'	"		"	"	"	....		
n-1	r(m-1,0)	r(m-1,m)	r(-2,1)	i(-2,1)	r(-2,2)	....		
n	i(m-1,0)	i(m-1,m)	r(-1,1)	i(-1,1)	r(-1,1)	....	r(-1,m-1)	i(-1,m-1)

Note: $r(m+1,1) \equiv r(-(m-1),1)$
$n \equiv N$

2.3 Time Stepping

As demonstrated above, the use of Fourier transforms converts the original partial differential equation on an $N_x * N_y$ grid to a coupled set of $N_xN_y/2$ partial differential equations in the complex spectral amplitudes (2.1.12). This section describes a suitable time stepping scheme for this solution.

Orszag (1971) warns that explicit foreward time stepping of the Jacobian term will be unstable. On the other hand, stability of the diffusion term contribution requires an implicit solution. A mixed leapfrog-implicit scheme satisfies these requirements:

$$\frac{\psi^{t+\Delta t} - \psi^{t-\Delta t}}{2\Delta t} = \frac{J^t}{k_m^2+\ell_n^2} - \nu(k_m^2+\ell_n^2)\left(\frac{\psi^{t+\Delta t} + \psi^{t-\Delta t}}{2}\right) \qquad (2.3.1)$$

which, rearranged, becomes

$$\psi^{t+\Delta t} = \frac{(1-\nu(k_m^2+\ell_n^2)\Delta t)\psi^{t-\Delta t} + 2\Delta t\frac{J^t}{k_m^2+\ell_n^2}}{1+\nu(k_m^2+\ell_n^2)\Delta t} \qquad (2.3.2)$$

To start from t = 0, first a prediction of $\psi^{\Delta t/2}$ is made, and then this is used to step to Δt:

$$\psi^{\frac{\Delta t}{2}} = \frac{(1-\nu(k_m^2+\ell_n^2)\frac{\Delta t}{4})\psi^0 + \frac{\Delta t/2\ J^0}{k_m^2+\ell_n^2}}{1+\nu(k_m^2+\ell_n^2)\Delta t/4} \qquad (2.3.3)$$

$$\psi^{\Delta t} = \frac{(1-\nu(k_m^2+\ell_n^2)\frac{\Delta t}{2})\psi^0 + \frac{\Delta t\ J^{\frac{\Delta t}{2}}}{k_m^2+\ell_n^2}}{1+\nu(k_m^2+\ell_n^2)\ \frac{\Delta t}{2}} \qquad (2.3.4)$$

This scheme is accurate to order Δt^2, but may lead to an instability due to separation of even and odd time levels. To counteract this, time levels are averaged after some number of time steps. Several schemes are available from which the following has been selected.

$$\psi^{t+\Delta t} = \psi^{t-\Delta t} + 2\Delta t\ J^t \qquad (2.3.5)$$

$$J^{t+\Delta t} = J(\psi^{t+\Delta t}, \nabla^2\ \psi^{t+\Delta t}) \qquad (2.3.6)$$

$$J^{t+\frac{\Delta t}{2}} = \tfrac{1}{2}(J^t + J^{t+\Delta t}) \qquad (2.3.7)$$

$$\psi^{t+\Delta t} = \frac{(1-\nu(k_m^2+\ell_n^2)\frac{\Delta t}{2})\psi^t + \Delta t\frac{J^{t+\frac{\Delta t}{2}}}{k_m^2+\ell_n^2}}{(1+\nu(k_m^2+\ell_n^2)\frac{\Delta t}{2})} \qquad (2.3.8)$$

2.4 Energy and Enstrophy

In the absence of dissipation, energy and entrophy are conserved except for errors introduced by finite time differencing. As a check for correct execution of the Orszag algorithm, and to determine that the time stepping interval is sufficiently small, we evaluate (with $k^2 = m^2 + n^2$)

$$\text{Energy}_{tot} = \tfrac{1}{2} \sum_k k^2 \psi\psi^* \qquad (2.4.1)$$

and

$$\text{Enstrophy}_{tot} = \sum_k k^4 \psi\psi^* \qquad (2.4.2)$$

Energy and enstrophy may be transferred among modes, and this is monitored by the

$$\text{Energy transfer (k)} = R_e(J^*\psi) \qquad (2.4.3)$$

and

$$\text{Enstrophy transfer (k)} = 2\, R_e(k^2 J^*\psi)$$

2.5 Spectral and pseudo-spectral calculations

The algorithm developed in Section 2.2 is fully spectral in the sense that all contributions from aliasing are eliminated. One might want to solve some problems for which this approach is not possible. Orszag (1971) gives the example of a cloud dynamics model in which the conditions that precipitation occur is naturally handled in physical space while advection and dissipation are effeciently treated in spectral space. For such situations, one may transform the needed quantities back and forth between physical and spectral space, and either accept the resulting aliasing errors or adopt a scheme such as is described by Orszag (1971) to partially reduce them.

Even in cases where full de-aliasing is possible, one might perform pseudo-spectral calculations in order to reduce the number of FFT's per time step in half. For some problems aliasing errors may be negligibly small (Orszag, 1972, Fox and Orszag, 1973).

3. IMPLEMENTATION AT THE INSTITUTE OF OCEAN SCIENCES

3.1 Hardware environment

A realization of the theory of Section 2 is done on a Floating Point Systems 190L array processor (AP) attached to a Univac 11/60 host computer. The array processor has 128 k bit words of main memory, 4 k words of table memory and some read only memory containing constants.

The UNIVAC acts as a scheduler, initiatizing the AP, controlling the time stepping, swapping results between host and AP memory, and offloading diagnostics for future reference. These diagnostics are output to a plotting program,

using the NCAR graphics package, including spectra, stream function and vorticity contours and time plots of relevant quantities.

The maximum grid size in the models is 128 x 128; this necessitates keeping some quantities in UNIVAC main memory and swapping within time steps. FFT routines require that the data arrays reside in a single page of AP memory (64 k words), and this limits grid size to 256 x 256. This would require the storage of all quantities in host memory which can be prohibitively expensive in host time.

3.2 Array processor calls

Most AP calls fall into one of three categories: a) data in or out of AP; b) the manipulation of vector quantities (addition, subtraction, multiplication of vectors) or vectors with sealers; c) 2^D array operations (FFT's).

Since our problem is 2^D, we must treat data as sometimes 1^D vector and sometimes 2^D, as required by the various AP calls. This requires special effort to "remember where we are" at all times, but presents no insurmountable problems and the "bookkeeping" is both efficient and transparent to the user.

3.3 Special considerations for 2^D FFT calls

The efficiency of the Orszag method depends upon the existence of the FFT, as demonstrated in Section 2. The storage order of spectral space values in relation to real space storage order is characteristic of any given 2^D FFT routine, and knowledge of this order is a prerequisite of the routine's use. We must not only initialize spectral space values correctly, but also must generate arrays of p, q and $p^2 + q^2$ used in calculating derivatives, and their storage order must match that used by the routine.

For a complete description of the interpretation of k space and the details of programming the FPS 190L, the reader is referred to ADVEX, Ramsden (1984), which also gives a complete detailed set of programs for one simulation, along with extensive comments on the optimization of vector FORTRAN for this sort of program.

3.4 Graphics output

3.4.1 Monochrome imaging

We have mated the output from the spectral simulation with the National Center for Atmospheric Research (NCAR) graphics package. This means that all plots conform to the style of other installations. The NCAR package is a "smart" set of routines and is flexible in the choice of diagnostics. Final results are sent to a CALCOMP plotter or displayed on a Tektronix graphics terminal.

3.4.2 Colour imaging

Computer routines have been written to send 2^D real space fields to a colour imager operated by the Remote Sensing group at the Institute of Ocean Sciences. By intercepting the models at every time step, it is possible to send a time series of 2^D fields to the imager. This feature has been used to make a movie of several cases of the simulations. Slides of individual frames from a colour monitor have been made. This provides a powerful descriptive method since stream function fields can be overlayed on passive quantities, permitting visualization of the physics of various situations.

4. DEVELOPMENT AT IOS

4.1 Development to the present

In this section, the historical development of the programs and methods by Interact Computing Services for the Institute of Ocean Sciences under various contracts is presented. Also included is a general guide to some of the uses made of these programs.

This is done for two reasons. The first is that readers may see the logical development of the routines and their options. The second reason is that potential users may determine the degree of complexity that they desire. Examples will be given where applicable. We will not delve into the detailed nature of the programming considerations. For a complete description of these problems and their solutions, see Ramsden, 1984.

The basic programs have undergone extensive development, testing and refinement in the past two years, a process which continues at present. The changes have been of two basic types.

Type one represents an increased capability, diagnostic, or enhancement. Type two represents special cases which have been run as subsets of type one programs. Table 2, the detailed evolution of these systems, is shown below.

Table 2. Evolution of the Programs

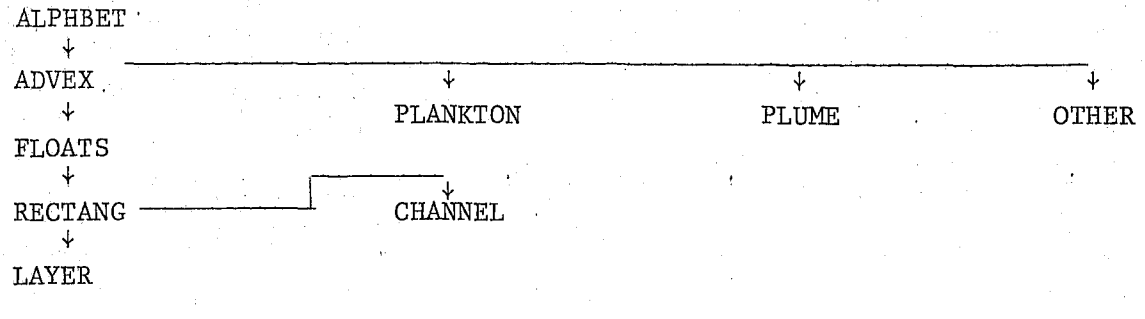

4.2 ALPHBET

The first program developed was ALPHBET, which solved only the equation

$$\frac{\partial}{\partial t}\xi + J(\psi,\xi) = D\xi \tag{4.1}$$

with

$$\xi = \nabla^2\psi. \tag{4.2}$$

For the development of this program, and a starting point for future developments, the work of Davey, 1980, and the computer programs of Haidvogel and Holloway (unpublished) were closely followed. The resultant process was one of freely translating Fortran code written for NCAR's CRAY-1 computer into F.P.S. array processor code.

This basic equation (4.1) allowed us to test the nonlinear parts of the eventual timestepping of equation (1.4), and we developed the basic timestepping method (2.3.1) subject to conservative properties (2.4.3) and (2.4.4), which sum to zero. This allowed us to lay out k space properly and work through the quirks of the array processor calls.

4.3 ADVEX

The next task was to develop the basic form of the advection diffusion equations

$$\frac{\partial}{\partial t}q + J(\chi,q) = F - Dq \tag{4.3}$$

with

$$q = (\nabla^2 - \alpha^2)\psi + h + \beta Y \tag{4.4}$$

and

$$\chi = \psi - \overline{U}Y \tag{4.5}$$

$$\frac{\partial}{\partial t}Q + J(\chi,Q) = g_y\frac{\partial\psi}{\partial x} - g_x\frac{\partial\psi}{\partial y} - DqQ \tag{4.6}$$

In these equations, β is the gradient of Coriolis parameter $\frac{\partial f}{\partial y}$, scaled to appropriate units (see Section 6), h is the elevation of bottom topographic features as a fraction of the mean depth and multiplied by the Coriolis parameter. This set of equations is one layer (barotropic). F is a random phase forcing operator with an energy distribution corresponding to some geophysically meaningful wave number spectrum. D is a dissipation operator

$$D\xi \equiv (A + B\nabla^2 + C\nabla^4)\xi \tag{4.7}$$

A corresponds to Ekman drag, which operates on all wave numbers. B is regular viscosity or Laplacian diffusion. C is a term sometimes called Biharmonic diffusion.

It is worth noting that in general, D and F will be prescribed for any long simulations which depend on statistical stationarity of the turbulence field.

The nature of 2 dimensional turbulence is for the advection operator to selectively move energy to low wave numbers, and enstrophy to high wave numbers (whilst maintaining the net sum of both). This effect has been likened to the tendency of rotating objects to tumble into their highest moment of inertia eigenstate (Thompson, 1983). To counter this, we apply a mixture of Ekman drag and a Laplacian or biharmonic dissipation, which selectively operates on higher wave numbers. To maintain energy levels, we apply forcing centered on a median wavenumber. By balancing forcing, dissipation and drag, a satisfactory statistically stationary state can be reached.

It is worth noting that the Laplacian and biharmonic operators can be thought of as moving energy and enstrophy to finer scales of motion which can not be resolved by the finite grid size of the model. One of the criteria for these operators is that they should produce a spectrum of energy which passes smoothly through the highest wavenumbers out to the unresolved scales.

Continuing with equation (4.3), q is the total potential vorticity in the fluid column and is equal to the sum of the relative vorticity, the surface displacement stretching term $\alpha^2\psi$, the planetary vorticity βY, and h, the relative topography scaled to units of vorticity. This last term represents the vorticity gained or lost when a fluid column contracts or expands over a piece of terrain.

In equation (4.4), α^2 is the square of the inverse Rossby radius of deformation.

χ is the total stream function and is equal to the local stream function ψ and a mean flow term. It is interesting to note that one of the capabilities of the model is to start with an initially quiescent stream function ψ and "blow" mean flow over some topography. An eddy field will develop.

In equation (4.6), Q is any passive scalar; passive in the sense that it does not interact with the flow field, and is merely swept around by the turbulence and mean flow. g_x and g_y represent the mean gradients of quantity Q in the x and y directions respectively. Dq is a diffusion operator on Q, equivalent in form to D.

With ADVEX, standard output was developed and diagnostics which may be printed and/or plotted at any timestep or timestep interval. In addition, time series of relevant diagnostics can again be printed or plotted. There are several restart options whereby the end states of one or more simulations can be used as beginning states of new simulations. One may choose to duplicate runs exactly or to randomize selected parts.

From the basic advection/diffusion equations we have generated several specialized subsets of programs.

4.3.1 Stirring of a passive tracer

Research has been done in which a passive tracer field, Q(x,y,t) is advected by the flow given by ψ as given by equation (4.6).

Here Q is perturbation concentration of, say, a dissolved chemical substance, (g_x, g_y) is any large scale mean gradient of concentration and Dq is some operator, to be specified, which acts to dissipate small scale fluctuations in Q. Such a model might then show how oceanic tracers are stirred along isopycnal surfaces by mesoscale eddies or large amplitude Rossby waves. One of the first goals is to see how homogeneous quasigeostrophic turbulence may be characterized by an "eddy diffusivity" acting on the tracer field. Figures 1a to 1d show some results from this study and are described in the figure captions.

4.3.2 Advection of a Plume

As another enhancement of ADVEX, consider a case where a turbulent field is moving past a fixed site from which a tracer leaks at a constant rate. Such an example might describe contaminant escaping from a seafloor radioactive waste dump site or the horizontal evolution of a hydrothermal vent plume. In the plume source field is a Gaussian spot, and we bring on a mean flow from the east over a topography. The topography consists of a random terrain plus a north/south ridge with the plume site on the crest of the ridge. This example clearly illustrates the breaking off of tongues of injected material, and the role of eddies in transporting material. See Figures 2a to 2k.

4.3.3 Evolution of error maps; predictability of quasigeostrophic turbulence

Weather forecasting and, increasingly, efforts at upper ocean forecasting are limited by a) inadequate theoretical and numerical dynamics, and b) lack of complete and accurate initial data and of accurate subsequent boundary conditions. Predictability studies attempt to assess the relative strengths of these limitations. Most predictability research has focused on propagation and amplification of forecast error in the wavenumber domain. We have begun a few studies concerning the physical configurations of error fields with respect to evolving flow structures. To do this, let us suppose that the dynamics embodied in equation (4.3) are "true". Then we ask how uncertainty in initial observations affects long term forecast accuracy. We may solve (4.3) twice, each flow evolving from initial conditions which differ in the smaller "unobservable" scales of motion. Taking the difference or "error" between two solutions, we seek to characterize error evolution in terms of the mean of two solutions. See Figs. 3a to 3d.

4.3.4 Topographic Interaction

This example elaborates the dynamics of the role of underlying topography in eqn. (4.3). Combining (4.3), (4.4) and (4.5) yields

$$\frac{\partial}{\partial t}(\nabla^2-\alpha^2)\psi + U\frac{\partial}{\partial x}(\nabla^2-\alpha^2)\psi + h \quad + J(\psi,\nabla^2\psi + h) = F + D \qquad (4.8)$$

Taking $\psi = 0$ at $t = 0$, equation (4.8) reduces to

$$\frac{\partial}{\partial t} (\nabla^2-\alpha^2)\psi + U \frac{\partial h}{\partial x} = 0 \qquad (4.9)$$

In this way, the topographic field h, in the presence of a steady zonal flow U, will generate eddy vorticity $(\nabla^2-\alpha^2)\psi$. As the flow evolves, correlations between meridional eddy flows $\frac{\partial}{\partial x}\psi$ and h generate a "topographic form drag" which may resist or even accelerate U.

As a note, the nature of h is such that the water column depth H can be given by

$$H = H_0(1-\tilde{h}(x)) \qquad (4.10)$$

where $\tilde{h}$ is nondimensionalized by the mean depth. The fractional change of vorticity by shrinkage or expansion of the water column by going over the topography is then

$$\frac{\partial \xi}{\partial t} = - f \frac{\partial H}{\partial x} U \qquad (4.11)$$

Then (4.11) into (4.10) gives

$$\frac{d\xi}{\partial t} = U \frac{\partial}{\partial x} h \qquad (4.12)$$

where $h = f\tilde{h}$

and h is now scaled to units of vorticity. Under investigation are the relations between U, the statistics of h and the resulting eddy field. Figures 4a to 4e show the results of one such simulation along with some useful diagnostics of the flow interaction.

4.3.5 Plankton patchiness

This is really only an extension of the stirring of a passive tracer described by eqn. (4.6). Consider the vertically integrated biomass of primary producers in the euphotic zone. Let C be the logarithm of area density of the integrated biomass. We wonder what controls the horizontal patchiness of C. A conjecture is that patchiness is largely a result of horizontal stirring. As a simple model for dynamical evolution of a horizontal transport streamfunction, consider (4.3). Suppose that C is advected as a passive but, nonconservative tracer. The simplest biological dynamics that we can assume are exponential growth and decay. Since C is already a log transform of biomass, the equation of motion is

$$\frac{\partial C}{\partial t} + J(\psi,c) = r + D_c \qquad (4.13)$$

where r is a growth decay rate coefficient and D_c is an operator which results in dissipation of C fluctuations at small scales. Note a point of ambiguity: should an "eddy diffusivity" act directly on the biomass concentration or on C?

For convenience we assume the latter.

The immediate goal of this research is to discover how the statistical distribution of r, together with statistics of ψ, determines the statistical distribution of C. In some cases we have let $r(\underline{x})$ be a steady field of prescribed wavenumber spectrum. This is seen in Figs. 5a to 5e.

In this example the growth term r is shown in Fig. 5b. The r field is only defined for wave numbers $2 < K < 4$ with a random phase for each r(k). Each time step, another unit of log plankton is added according to r. The result is the "streakiness" exhibited by Figures 5c and 5d.

We also include Fig. 5e, a useful diagnostic of the field, the scalar variance transfer, which is defined as

$$T(\phi) = \text{Real} \quad \phi \cdot J^*(\psi,\phi) \tag{4.14}$$

The transfer $T(\phi)$ is integrated over $|k|$ and Figure is the result. This figure shows that material is removed from wave numbers $2<K<4$ (the wave numbers we are injecting at), and distributed to higher wave numbers. By examining sequences of diagnostics such as these, things such as statistical stationarity can be determined.

4.3.6 Stirring by an isolated eddy

In Figures 6a to 6d we show the time evolution of a Gaussian spot of turbulence generation perturbation scalar from a mean gradient of scalar in the Y direction. As the flow evolves, the spot "wraps up" the perturbation scalar.

4.3.7 Diffusion effects

There is some disagreement among oceanographers as to the correct form of the dissipation operator to apply in equations (4.3) and (4.6).

A study has been undertaken in which the direct effects of $B\nabla^2\xi$ and $C\nabla^6\xi$ are compared. A Gaussian spot of dye is released on top of a Gaussian spot of turbulence on a β plane. Figures 7a and 7b show the time evolvement of two cases. Fig. 7a utilizes Laplacian or harmonic dissipation and Fig. 7b utilizes biharmonic dissipation. To produce comparable results, B and C are chosen to have equal Batchelor wavenumbers K_β.

Clearly shown are the differences ∇^2 dissipation makes from ∇^4 dissipation.

Also note the negative contours in the last of 7b. One of the limitations of the spectral method is that negative quantities can be generated near steep gradients of that quantity, and the requirement of positive definite quantity can be violated.

4.4. FLOATS

A further enhancement of ADVEX is the addition of Lagrangian particles, FLOATS. This entailed finding the values of the stream function, velocity, or

other quantity at non grid points. A thorough investigation and testing of various methods to do this was conducted. One method is to do a slow Fourier transform on the requisite fields, but this proved to be too slow. A faster method was found to consist of a fast Fourier transform followed by a real space interpolation over some region near the required point, taking advantage of the periodicity at the edges. This also has the advantage that one FFT will suffice for any number of points desired. The complete analysis of the Float method will be developed in Section 7.

The interpolation formula is given thusly. If x and y are the desired points to find a field Φ, x,y not a grid point, then

$$\Phi_{(x,y)} = \sum_{i=1}^{m} \sum_{K=1}^{m} A_{i_K} \prod_{\substack{j=1 \\ j\neq i}}^{m} \prod_{\substack{\ell=1 \\ \ell\neq K}}^{m} (x-x_j)(y-y_\ell) \tag{4.15a}$$

$$A_{i_K} = \Phi_{i_K} \left[\prod_{\substack{j=1 \\ j\neq i}}^{m} \prod_{\substack{\ell=1 \\ \ell\neq K}}^{m} (x_i-x_j)(y_K-y_\ell) \right]^{-1} \tag{4.15b}$$

where x_j and x_i, y_k and y_i are grid point values, m is an order of fit, and Φ_{ik} is the value of the function at (x_i,y_k).

It was found that m = 4 gives a reasonable fit.

To timestep the floats, a predictor/corrector method was developed. This development provides a powerful tool which has been used to study different things such as straining in different flow regimes.

A large suite of float diagnostics has been developed, such as statistics of float pair separations, and lagged autocorrelation of velocity fields with estimates etc.

4.4.1 Floats in a turbulent regime

Figures 8a through 8f show the results of two experiments. Floats in Fig. 8a are released into a turbulent regime without β, 8b are released near the same spots in the same <u>initial</u> turbulence field, but with β.

Only some of the float pairs (randomly orientated with respect to each other at t = 0) are plotted in Fig. 8a. Fig. 8b shows clearly the tendency for floats to travel east/west in the presence of β. Figures 8c to 8d show the average distance away from the initial drop site for all floats. Periodicity is removed from these calculations. Figures 8c and 8e show the average X direction pair separation.

Figures 8d and 8f show the same statistics for the y direction. The presence of β is clearly delineated in quantitative terms.

4.5 RECTANG

The next enhancement was to go from a square to a rectangular k space domain and at the same time allow x to range from 0 to R 2Π in real space where R is any number, not necessarily 1. This meant some fundamental alterations to the dealiasing of the advect operator, going from a circular to an elliptical truncation of k space. k space had to be redefined to account for the factor R. This new program was called RECTANG.

As a special case of RECTANG, CHANNEL was developed in which side walls are placed at y = 0, Π(R) in a free slip condition. This implies no flow across the barrier since $U_y = \frac{\partial \psi}{\partial x} = 0$. By doing this, one half of our real space is lost since $\psi(y) = -\psi(-y) = -\psi(2\Pi - y)$. This also implies ½ of k space is lost and it is fairly easy to show that

$$\psi(y) = -\psi(2\Pi - y) = \psi(k_x, k_y) = -\psi(k_x, -k_y) \tag{4.16}$$

This enhancement meant some changes, and the mixing and forcing must also maintain the channel condition.

4.6 LAYER

The last development brought on line at present is program LAYER, in which the method is extended to incorporate baroclinicity. The one layer system has been extended to two layers but the capability to easily extend the programs to three or more layers is available. For any multi-layer systems, the governing equations are, C.F. Pedlosky, 1979, Pg's. 386 to 393

$$\frac{\partial}{\partial t} q_i + J(\chi_i, q_i) = F_i - D_i \tag{4.17}$$

with

$$q_i = \nabla^2 \chi_i + \Lambda_{ij}(\chi_j - \chi_i) + \Lambda_{ik}(\chi_k - \chi_i) + h_i + \beta Y \tag{4.18}$$

$$\chi_i = \psi_i - \bar{U}_i\, y \tag{4.19}$$

These are the equations for a multi-layer system. Equation (4.3) has been modified to satisfy each layer individually and has become equation (4.17), equation (4.4) has been modified for the coupling effect of the layers above and below the layer i, and becomes equation (4.18). In equation (4.18), the α^2 term of equation (4.4) is now $\Lambda_{ij}(\chi_i - \chi_i)$, where Λ_{ij} links the layer i to the layers above and below it by the effect of surface displacements and gravity.

$$\Lambda_{ij} = \frac{\alpha^2_{ij}}{R_i} \tag{4.20}$$

In equation (4.20), R_i is the fraction of the water column in layer i, i.e. $R_i + R_j = 1$. α^2_{ij} is explicitly given as

$$\alpha^2_{ij} = \frac{f_o^2 L^2}{g|\rho_i - \rho_j|/\rho_o} \tag{4.21}$$

where f_o is the inertial frequency, L is a length scale of the motion, g is gravity and $|\rho_i - \rho_j|/\rho_0$ is the density contrast between layer i and layer j.

Going back to (4.20), h_i is the topography associated with layer i, generally zero except for the bottom layer.

In equation (4.19), we note that each layer can have a different mean flow. One of the features of baroclinic turbulence is an ability to generate eddies purely from a difference in the mean flows between layers, provided some initial perturbation exists.

There are some difficulties associated with going to a multi-layer system, the chief of which is the increased computer storage needed because the layers ψ_i are coupled by equations (4.17)-(4.19).

The two layer model has been tested thoroughly for such things as baroclinic Rossby waves, energy conservation, etc.

In program LAYER, an extra scalar field has been added for each layer, and the Lagrangian float section has been modified to include any number of floats in each layer.

4.6.1 Flow in a layered environment with sidewalls.

In Figures 9a to 9d a baroclinically unstable case is run in the presence of side walls to illustrate various developments.

In this example, 2 random turbulence fields are initialized with the upper layer being more energetic than the lower. A drag term is imposed on the lower layer to simulate energy loss by friction at the bottom.

Baroclinic instability is possible in a two layer system, (see Pedlosky, 1979) when effective $\hat{\beta}$ defined by

$$\hat{\beta} = \beta - \Lambda_{ij}(U_i - U_j) \tag{4.22}$$

has a different sign in each layer. In this way the system is expected to behave as a baroclinically unstable system subject to the side walls constraint.

Shown are two sets of plots. The lower layer stream function and the difference stream function which acts as a potential energy term for the evolving fields.

Although we have no immediate intentions to investigate these baroclinic flows, a couple of problems might be mentioned. A study of baroclinic flow above irregular topography could be performed with the goal of clarifying the role that bottom topography plays in maintaining the mean baroclinicity of

ocean currents. Perhaps more interesting is the question of horizontal heat transport in a baroclinic eddy field; a closely related problem is that of vertical momentum transport in a baroclinic eddy field. Adequate parameterization of these effects will be necessary to success of world ocean circulation simulations as appropriate to climatic studies.

5. CURRENT DEVELOPMENT

As mentioned previously, the applications described above just happen to be the first uses we have made. How we wish to emphasize the versatility, as well as high accuracy and efficiency, of the method.

5.1 Internal wave dynamics

As rather a different problem, we will investigate interactions among large amplitude internal waves. An idealization, which here is severe, is to restrict all motion to lie in a vertical plane. Because of the anticipated importance of interactions among disparate scales, it is necessary to concentrate computer resolution into a vertical plane. Nonetheless, many of the outstanding and sharply debated questions of internal wave - wave interaction theory can be resolved within the vertical plane idealization. The problem can be posed in terms of a scalar vorticity field and a density field which are cross-coupled by gravity and the mean density gradient.

Future work will use this method to study breaking internal waves in which Q, the scalar field, will now be a buoyancy field. This field will interact with the turbulence field by

$$\frac{\partial}{\partial t}\xi + J(\psi,\xi) = g\frac{\partial Q}{\partial x} + D\xi \qquad (5.1.1)$$

g is gravity

For this sort of model, the model will be turned on end X|Z rather than x,y so there will be no β or h terms. The $g\frac{\partial Q}{\partial x}$ term in (4.15) comes about because a gradient of Q in the x direction will result in a source of vorticity when gravity attempts to move the neighbouring particles to their rest positions. i.e.

$\frac{\partial v}{\partial x} \neq 0$. Since $\xi = \frac{\partial u}{\partial y} - \frac{\partial v}{\partial x}$, we see that even an initially quiescent vorticity field will evolve under the interaction with buoyancy.

Figures 10a to 10d show the evolvement of a sport of buoyancy released into an initially quiescent turbulence field.

5.2 Double diffusive instability

On account of growing interest in, and appreciation of the importance of, double diffusive instability (DDI), an initiative has been made to begin a numerical investigation. The problem, as with internal wave dynamics, will be posed in vertical plane idealization (to be accompanied by limited 3^D simulations). Density will be determined linearly by two fields, say heat and

salt, of markedly different diffusivities. Goals of research will be to characterize heat and salt fluxes under conditions of fully developed DDI. We will seek to clarify the morphology of developing DDI, such as detachment of salt fingers. An area of novel physics to explore will be the role of internal wave straining in modulating DDI.

5.3 Imposition of irregular boundaries

A clear limitation of spectral simulations is that fluctuating quantities need to satisfy periodic boundary conditions. More restrictive conditions may certainly be imposed, such as no flow or free slip on rectangular boundaries (since this is a subset of the periodicity condition). However, it could be desired to accomodate conditions imposed along an irregular boundary such as a coastline. It appears that this can be accomplished by means of a so-called "capacitance matrix" method. Such a development could be useful for coastal dynamics studies and also would represent a fundamental contribution to numerical fluid dynamics.

5.4 Three Dimensions

We are moving in the direction of the simulation of 3 dimensional flow, which would involve solving the Navier Stokes equations (1.1) to (1.3) directly. This will involve a totally new approach in which we will abandon the stream function and keep a 3 dimensional velocity field instead subject to incompressibility. As a start to this capability, we have written and tested an algorithm to compute a 3 dimensional fast Fourier transform, both forward and reverse.

6. SCALING OF REAL WORLD PARAMETERS

As an insight into the practicalities of the methods, we include here a section on transforming computer scales to oceanographic or meteorological scales or vice versa. Our computer grid is of nominal length $2\Pi = \ell_c$. If we wish to model a 1000 km x 1000 km grid, $= \ell_0$ then the length ratio is $L = \frac{\ell_0}{\ell_c} = \frac{10^6 m}{2\Pi} \approx 1.5 \times 10$ m. Our computer time tc is dimensionless = 1.0. A representative time scale for geostrophic motion in the open ocean is about a month = 3×10^6 sec = t_o time ratio

$$T = \frac{t_0}{tc} = 3 \times 10^6 \text{ sec}$$

An average velocity for the mid ocean V_o is 7 cm/sec. Converting this to computer units, we get

$$v_c = v_0 \times \frac{T}{L} = \frac{07m}{sec} \alpha \frac{3 \times 10^6 sec}{1.5\ 10^5 m} = 1.4$$

This represents an rms velocity in computer units. We would initialize the model with an energy = $\frac{1}{2}V_c^2 = \frac{1}{2}(1.4)^2 \approx 1$.

To calculate β_c, we would get for a mid-latitude β_0

$$= \beta_0 \text{ of } 2\times10^{-11} \text{ m}^{-1} \text{ sec}^{-1}$$

$$\beta_c = \beta_0 LT = 2\times10^{-11} \text{ m}^{-1} \text{ sec}^{-1} \times 1.5\times10^{5}\text{m} \times 3\times10^{6} \text{ sec} \simeq 10$$

For a Rossby deformation radius of 50 km = α_0^{-1} we would get for α_c

$$\alpha_c^{-1} = \alpha_0^{-1}/L = \frac{5.0\ 10^4}{1.5\ 10^8} \simeq 1/3 \quad \alpha = 3$$

With proper care, real world examples are thus seen to be represented by computer units.

7. QUALITY CONTROL

At every stage of development, a thorough attempt has been made to prove model results. This section outlines some of the numerical and analytical tools that have been used to test the accuracy of the numerical methods.

7.1 Roundoff error

The F.P.S. system uses a 38 bit word of which 24 bits are mantissa. To test for roundoff error, there were few runs which duplicated simulations with 16 bit mantissas by randomizing the last eight bits. No significant differences were observed between the runs after a few hundred timesteps.

7.2 The advection operator

Already mentioned is the fact that energy and enstrophy transfers should sum to zero.

As a corollary of this, in the absence of forcing or dissipation, there should be no change in the total energy or enstrophy in timestepping the advect operator on the stream function field.

Scalar variance Q^2 in the absence of diffusion sources g_x and g_y should also be conserved by advection. These have been tested.

7.3 Wave propagation

By omitting the advection operator, (4.3) reduces to a simple form

$$\frac{\partial}{\partial t}\psi = \frac{ikx\beta^{\psi}}{k2} \qquad (7.1)$$

here $\overline{U}$,h,D,F = 0

by running the model in this way, $\frac{\partial}{\partial t}\psi(r)$ was tested against the analytical expression $\frac{ik_x\beta\psi(k)}{k^2}$.

7.4 Floats

Tracking of Lagrangian particles, whose positions may not coincide with the regular grid points, poses a difficult problem requiring detailed analysis.

Any method or methods chosen must advance the positions of Lagrangian particles accurately without sacrificing speed of execution.

Three basic methods were considered.

1) Slow Fourier transform of the requisite fields.
2) Real space interpolation (eqn. (4.7), (4.8)) of the fields.
3) For velocities, use a ψ field and differentiate; eqn. (4.7) with respect to x and y to set $U_x = -\frac{\partial\psi}{\partial y}$ explicitly, and likewise $U_y = \frac{\partial\psi}{\partial x}$.

There are several conservation properties which can be exploited.

1) An evolving stream function field conserves potential vorticity on a moving particle, in absence of forcing or dissipation.
2) If the stream function does not evolve, floats should trace closed orbits around constant stream function lines. Property 2 was chosen to rigorously test the approaches. 50 floats placed at random were advanced using various interpolations and slow Fourier transforms in frozen stream function fields exhibiting k^{-1} and k^{-3} behaviour. Also included was a suite of runs done with the top half of wave space truncated. Table 3 shows the relative execution times of the methods, and Table 4 shows the errors of the interpolation methods relative to the slow Fourier transform method.

Table 3. Methods of Float Positions

Relative Times Method	Time (arbitrary)
Slow Fourier Transform	3.7
4 Point Interpolation	.30
6 Point Interpolation	.97
8 Point Interpolation	2.23

Table 4. Relative Errors of the Interpolation Method

	Error	k^{-3} spectrum	Error	k^{-1} spectrum
Order of Fit	Not Truncated	Truncated	Not Truncated	Truncated
2	.589 E-2	.454 E-2	.273 E ϕ	.897 E-1
4	.198 E-2	.595 E-3	.173 E ϕ	.187 E-1
6	.138 E-2	.152 E-3	.135 E ϕ	.540 E-2
8	.111 E-2	-	.114 E ϕ	-

Method 3) was found to be twice as slow as method 2) and to give no better results.

The problem of time stepping was then included. To test the vorticity conservation, the following scheme was adopted. First

$$\bar{x}'(t+\Delta t) = \bar{x}(t) + \bar{V}(t)\Delta t \tag{7.5}$$

was calculated and then calculate $\bar{V}'(t+\Delta t)$ based on $\bar{x}'(t+\Delta t)$ and finally

$$\bar{x}(t+\Delta t) = \bar{x}(t) + \tfrac{1}{2}\{\bar{V}(t) + V'(t+\Delta t)\}\Delta t \tag{7.6}$$

The advancement of the vorticity, along with its dissipation was followed. Particles were then tracked and the vorticity and dissipative losses were recorded at each time step. Summing these dissipative losses and adjusting the measured vorticity, gave a diagnostic vortex following. Interpolations of 4 and 6 points using methods 2) and 3) were tried, and all methods gave average errors of 5% after 10 inverse rms vorticity times.

As a final test $V'(t+\Delta t)$ was calculated on the unadvanced stream function, but this gave no discernible change to the results.

7.5 Baroclinic flow

Two layer baroclinic flow has been implemented explicitly as to top and bottom layer. This gives us a suite of conservation properties to test.

a) Barotropic modes Rossby waves propagate as in (7.4). The layer stream functions are equal.

b) Baroclinic modes propagate at their correct phase speeds (Pedlosky, 1979, page 395).

$$\frac{\partial \psi(\bar{k})}{\partial t} = -\frac{i\beta K_x}{(k)^2+\Lambda_1+\Lambda_2}\,\psi(\bar{K}) \tag{7.7}$$

when $A_1 R_1 = A_2 R_2$

where R_1 is the fraction of water in layer 1
A_1 is the amplitude of layer 1
R_2 and A_2 are the same for the layer 2

Λ_1 and Λ_2 are determined by eqn. (4.20).

c) Total energy of the system is conserved by advection or wave propagation. In the absence of forcing or dissipation or H

$$\frac{\partial}{\partial t}\,\varepsilon_T = \frac{\partial}{\partial t}\,\frac{R_1}{2}|\nabla\psi_1|^2 + \frac{R_2}{2}|\nabla\psi_2|^2 + \frac{\alpha^2}{2}(\psi_1-\psi_2)^2 = 0 \tag{7.8}$$

$\frac{\alpha^2}{2}(\psi_1-\psi_2)^2$ is a potential energy term

α^2 is defined by equation (4.2).

d) In the absence of forcing or dissipation of H, layer enstrophy is conserved

$$\frac{\partial}{\partial t}\left\{\nabla^2\psi_1 + \Lambda_1(\psi_1-\psi_2)\right\}^2 = 0 \qquad (7.9a)$$

$$\frac{\partial}{\partial t}\left\{\nabla^2\psi_2 + \Lambda_2(\psi_2-\psi_1)\right\}^2 = 0 \qquad (7.9b)$$

REFERENCES

Davey, M.K. 1980. Numerical calculation of the spectral representation of $\underline{u}\cdot\nabla x$ for doubly periodic flow. Dept. of Oceanography, Univ. of Washington. Special Report No. 93.

Fox, D.G. and S.A. Orszag. 1973. Pseudospectral approximation to two-dimensional turbulence. Journal of Computational Physics 11: 612-619.

Orszag, S.A. 1971. Numerical simulation of incompressible flows within simple boundaries. I. Galerkin (spectral) Representations. Studies in Applied Mathematics 50: 293-327.

Orszag, S.A. 1972 Comparison of pseudospectral and spectral approximation. Studies in Applied Mathematics 51: 253-254.

Patterson, G.S. Jr. and S.A. Orszag. 1971. Spectral calculations of isotropic turbulence: efficient removal of aliasing interactions. Physics of Fluids 14: 2538-2541.

Pedlosky, J. 1979. Geophysical Fluid Dynamics. Springer-Verlag. 624p.

Ramsden, D. 1984. Program ADVEX. Details of implementing barotropic vorticity equations in Fortran. Interact Computing Services, Private Publication.

Thompson, P.D. 1983. "A Simple Mechanical Analogue of Two-Dimensional Flow", Journal of Correct Oceanography. Vol. 2, No. 1.

THIS PAGE IS BLANK

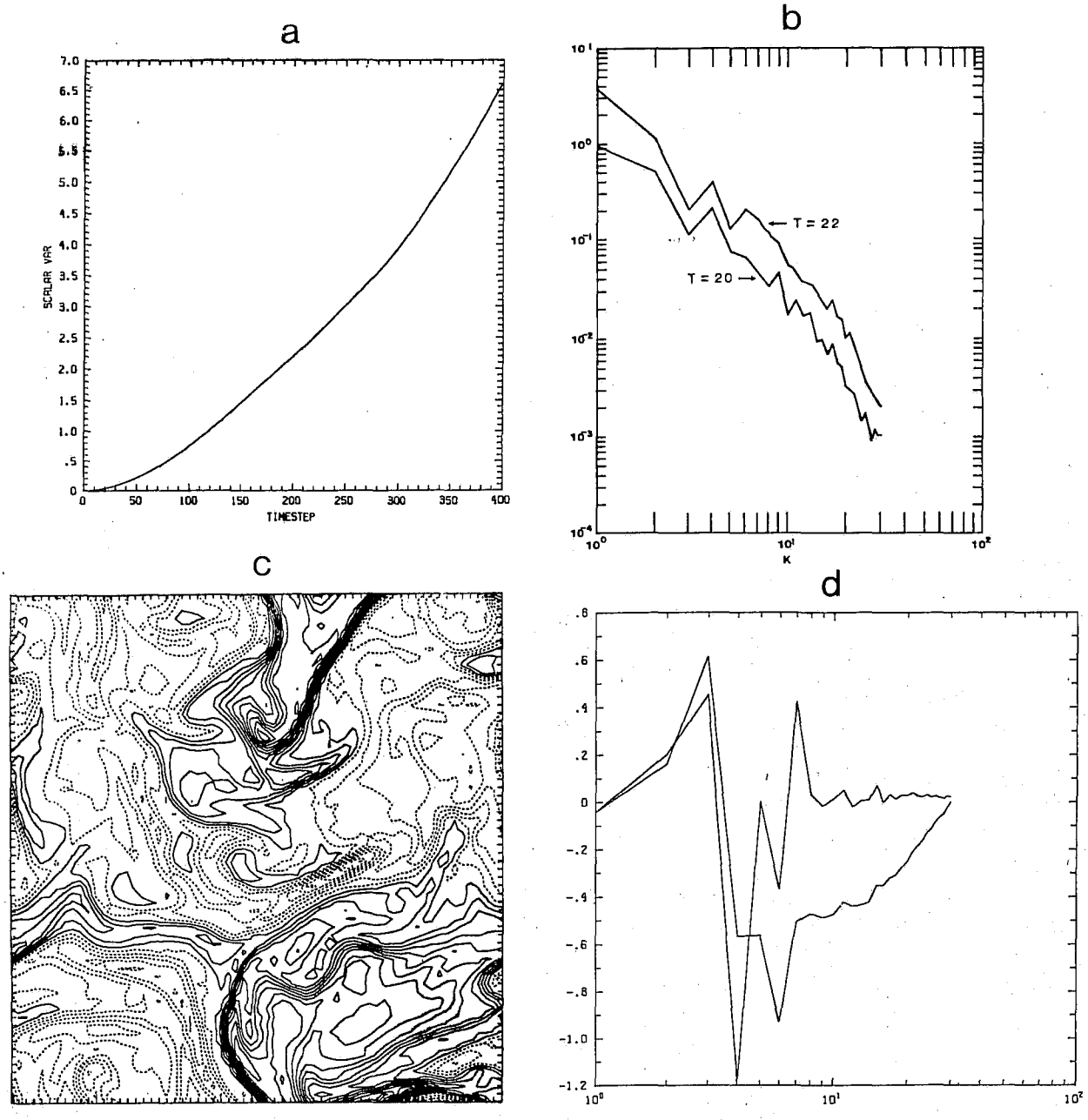

Fig. 1. This example shows the generation of an anomaly scalar field by the interaction of a turbulence field with mean scalar gradients in both the X and Y directions. This could represent the generation of a plankton nutrient field. Fig. 1a shows the time evolution of the net anomaly scalar Q^2. After some time, diffusion will balance generation of Q and the tendency for this to happen and generate a stable Q spectrum is shown in Fig. 1b. Fig. 1c is a real space picture of the Q field at t = 22. Fig. 1d shows a diagnostic of the turbulence field, the enstrophy spectra, and the integral of the enstrophy spectra versus wave number.

Fig. 2. In this example, a 'Juan de Fuca type' plume site on an oceanic ridge is simulated. Fig. 2a shows the topography h, used in this example. To an abyssal plain, random phase features are added and a ridge running in the Y direction centered at x = 2. The plume site, marked by an ⊛ is located on the crest of the ridge at Y = Π. Fig. 2b shows $h + \beta Y$, the effect of topography and β on turbulence. Fig. 2c shows the "spot" used to generate scalar quantity. It is to be thought of as a continuous releaser of some material. Figures 2d through 2g show the time evolution of total stream function $\psi + \beta Y$. Water movement will tend to be along lines of $\psi + \beta Y$. Figures 2h through 2k show the dispersal of ejected material at the same times as 2b through 2g. Note how material can be broken off or wrapped back. Many simulations such as this can be used to evaluate the statistics of plume dispersal.

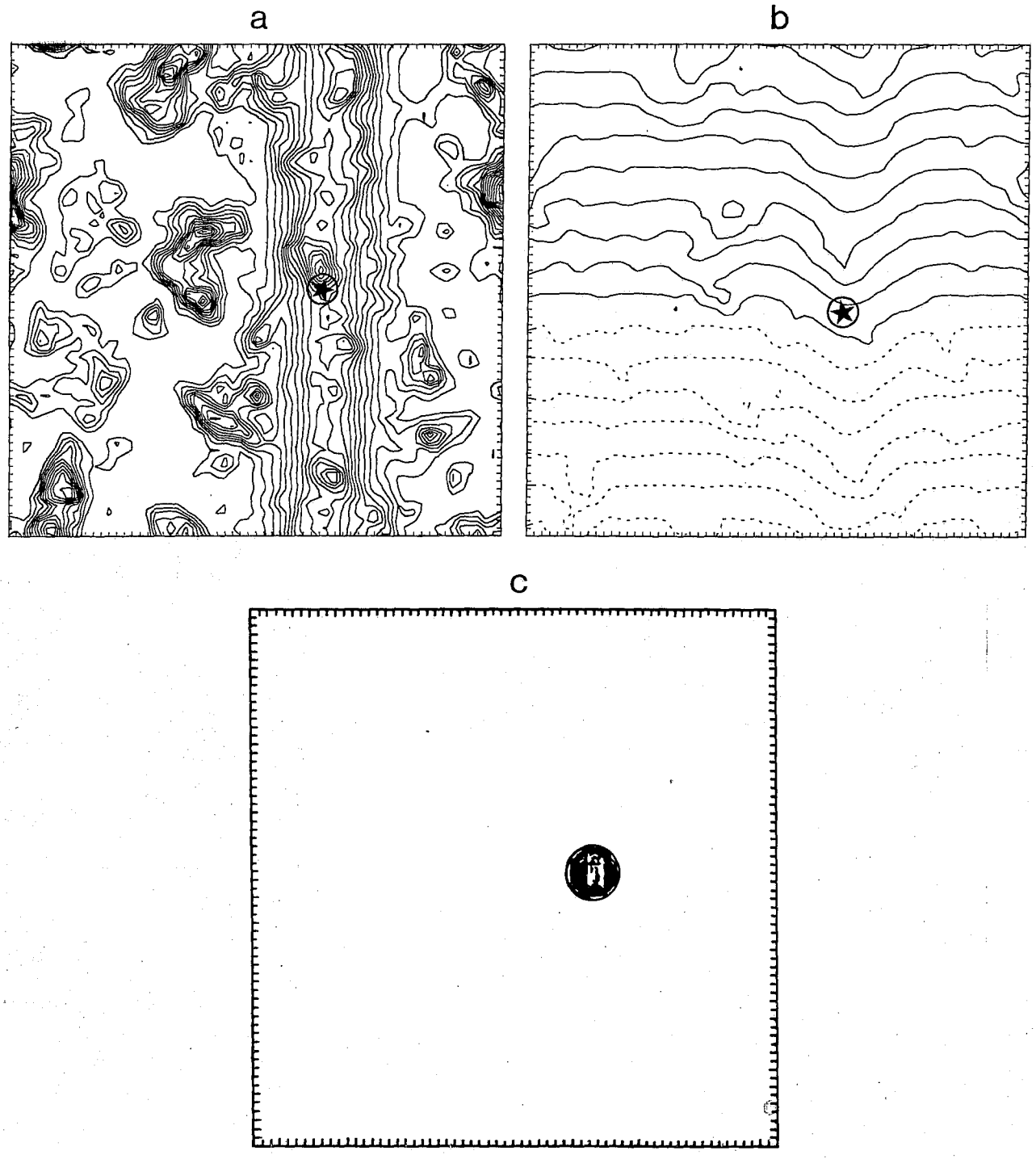

Fig. 2

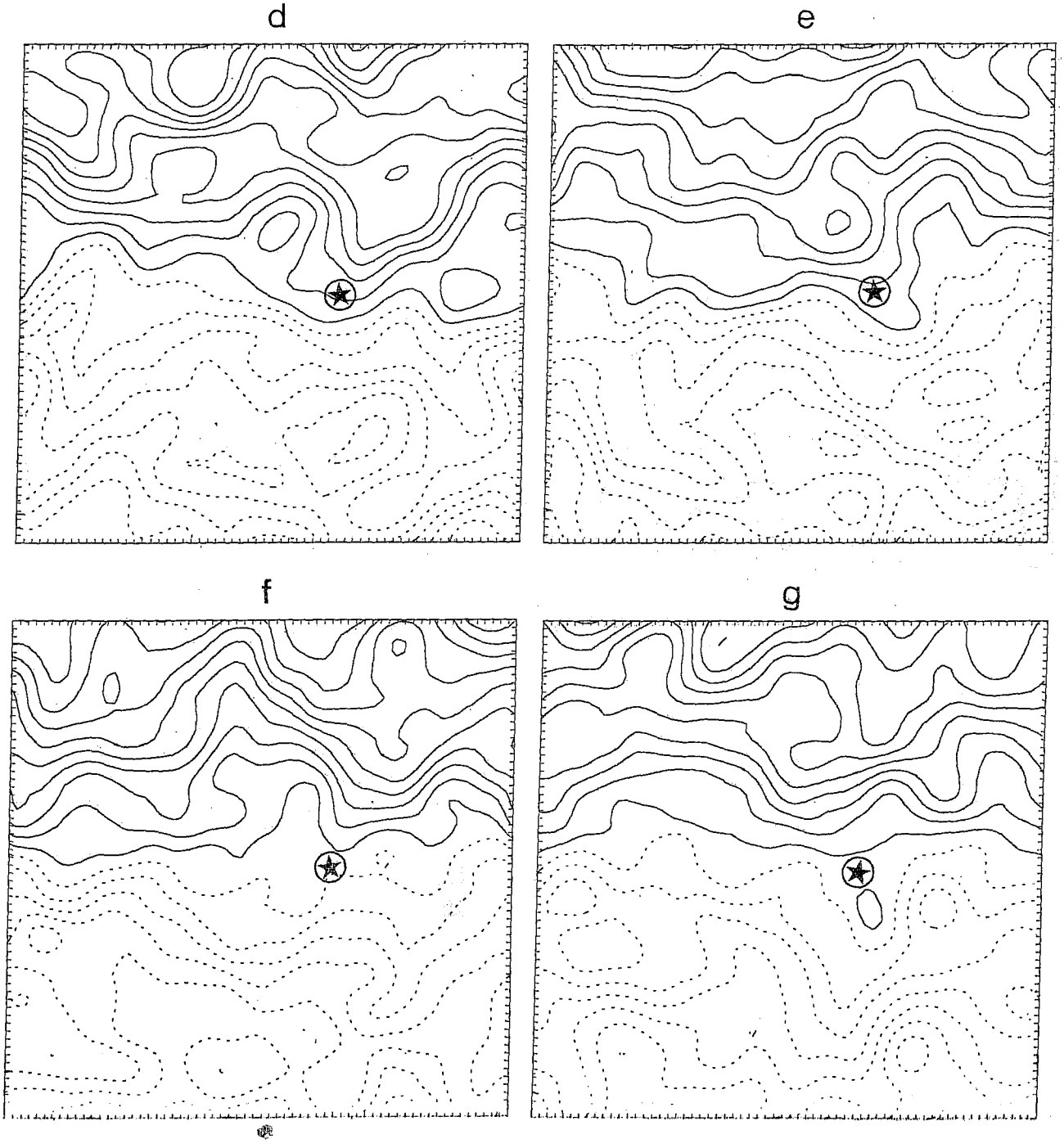

Fig. 2

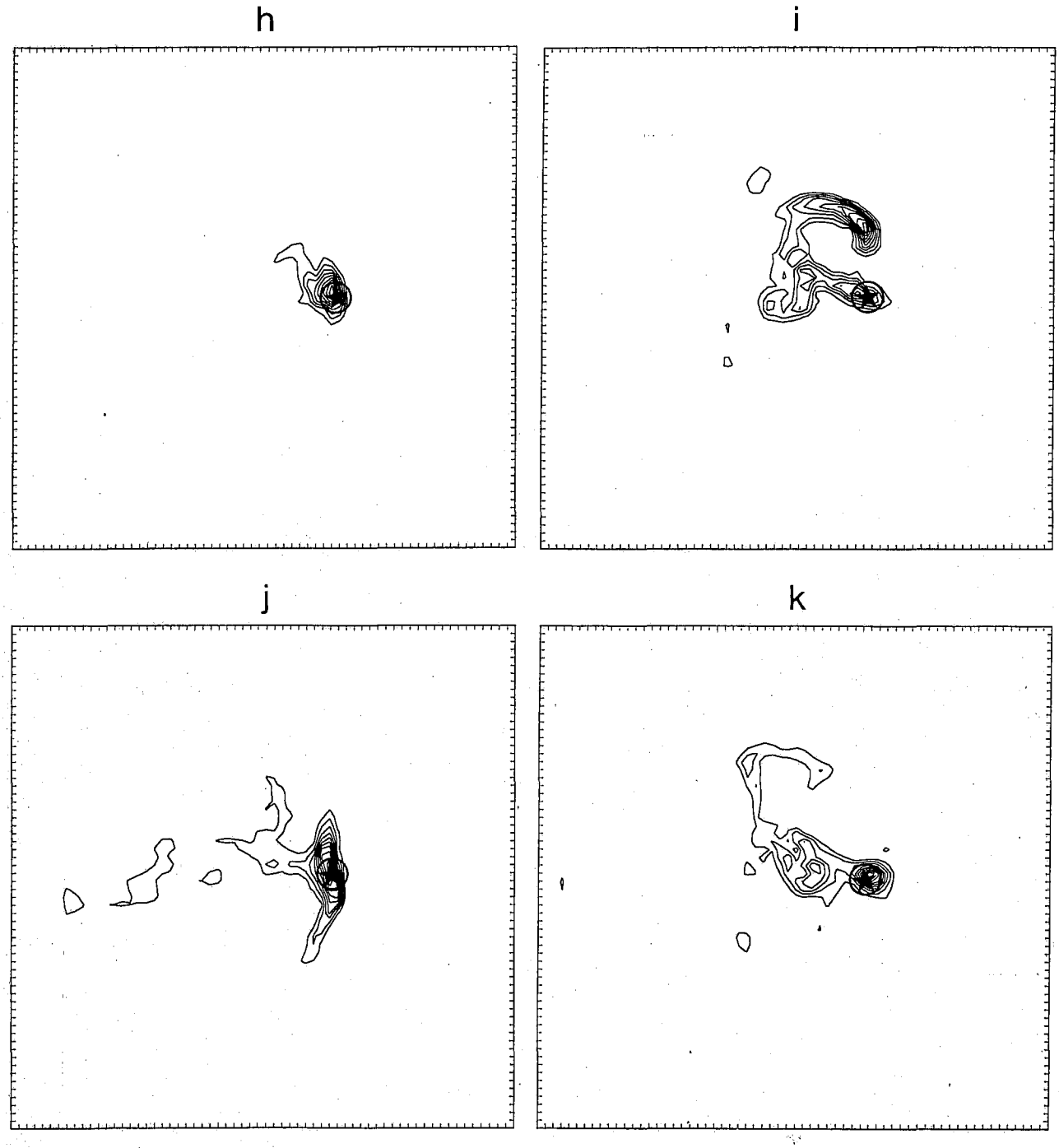

Fig. 2

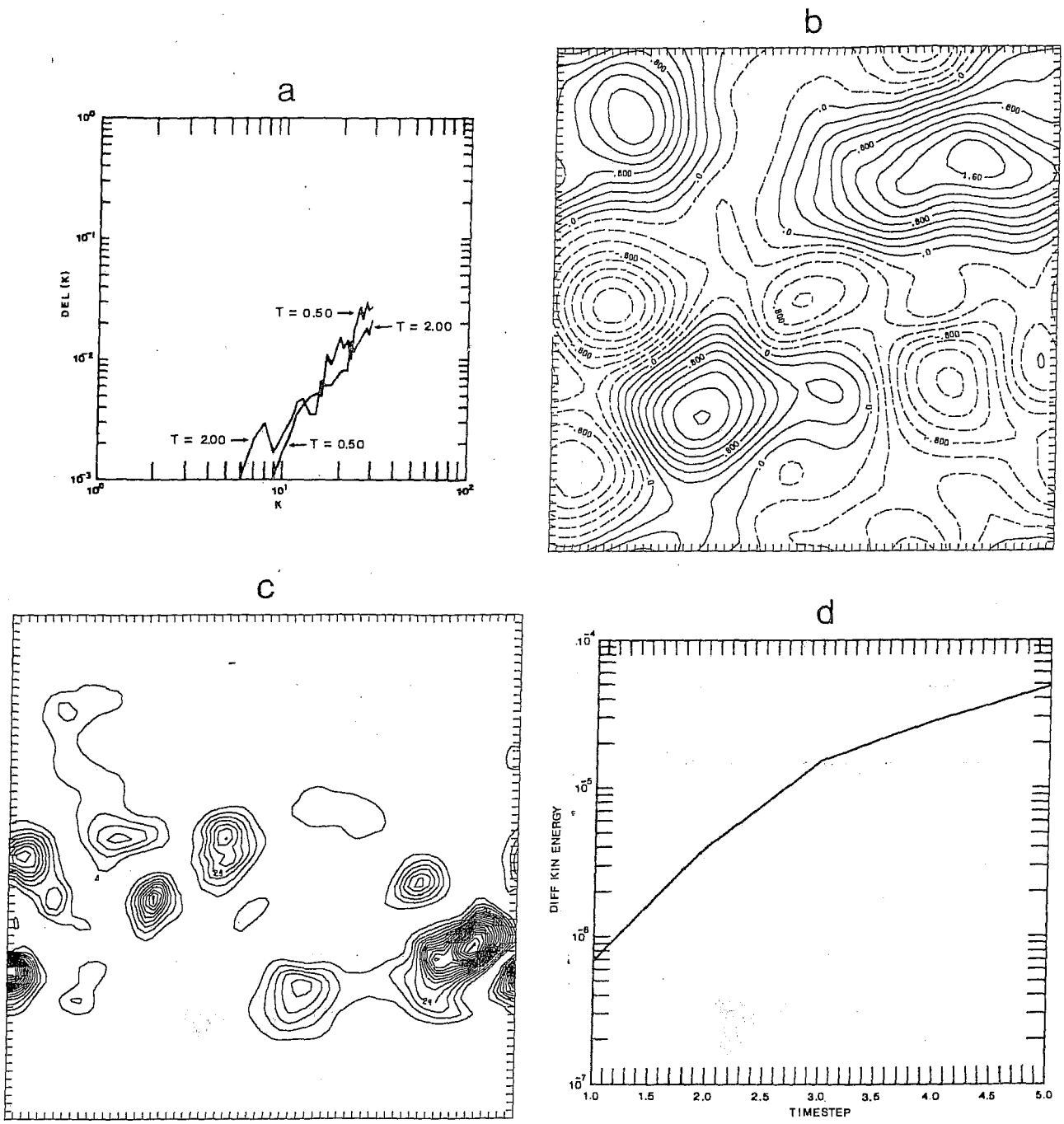

Fig. 3. This example shows the evolution of error as described in the text. Fig. 3a shows how the error has moved down to lower wavenumber at t = 2. At t = 0, only differences were at k > 25. Figure 3b is a picture of the average stream function $(\psi_1 + \psi_2)/2$ at t = 2. Figure 3c is a picture of $\delta^2 = (\psi_2 - \psi_1)^2$ after t = 2. Note the localization of error near the bottom right of the picture. Figure 3d is a time series of the difference energy $\frac{1}{2}K^2(\psi_2 - \psi_1)^2$, summed over all K.

THIS PAGE IS BLANK

Fig. 4. In this example, mean flow generates a turbulence field over a topography. Fig. 4a shows the topography used in this example. The mean flow is to the east, and after one time unit, the stream function field, Fig. 4b, has been generated. Fig. 4c shows the growth of total kinetic energy in the simulation. If dissipation is included, this quantity will eventually reach statistical stationarity. Fig. 4d shows the enstrophy transfer at each wave number K at t = .25. This is $\sum_k$ Real $k^2(H^* \cdot \psi)$. Fig. 4e shows $(V \cdot H)$, the velocity times topography, another useful diagnostic of the generated ψ field.

a

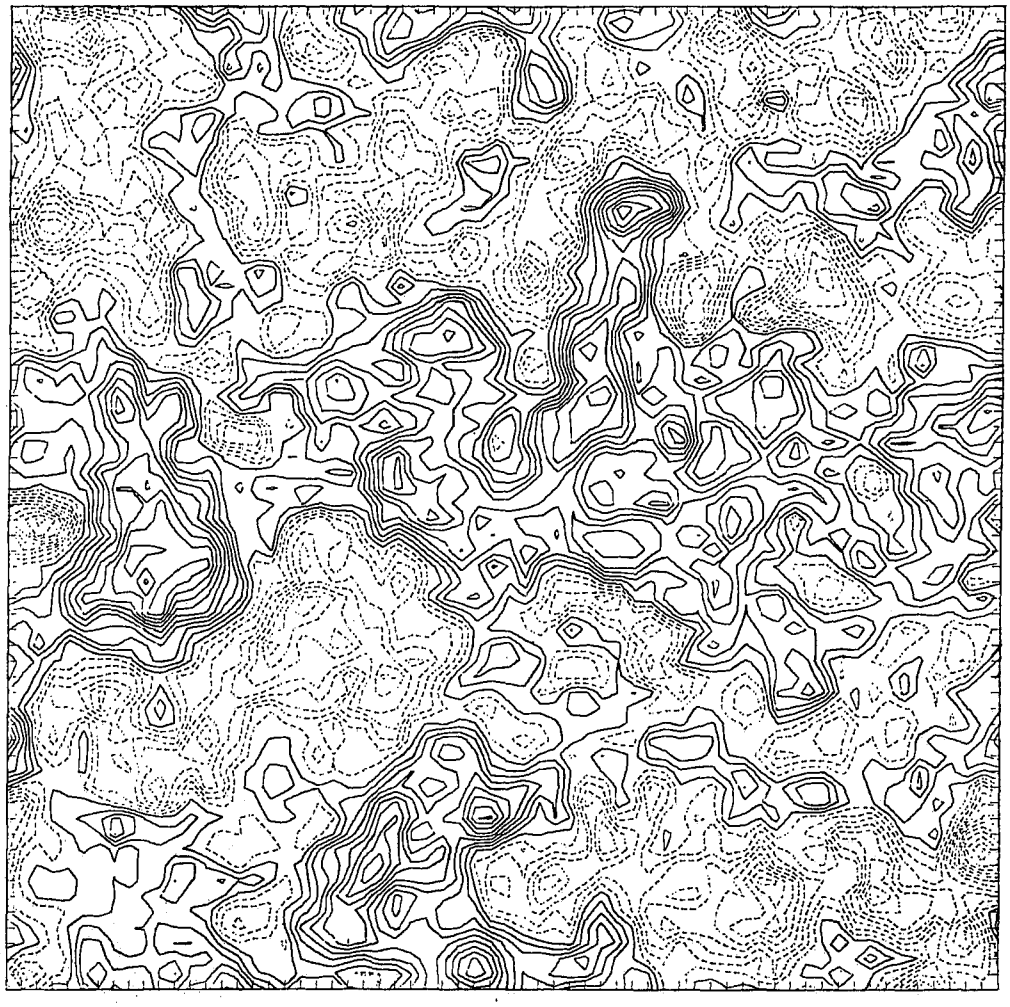

Fig. 4

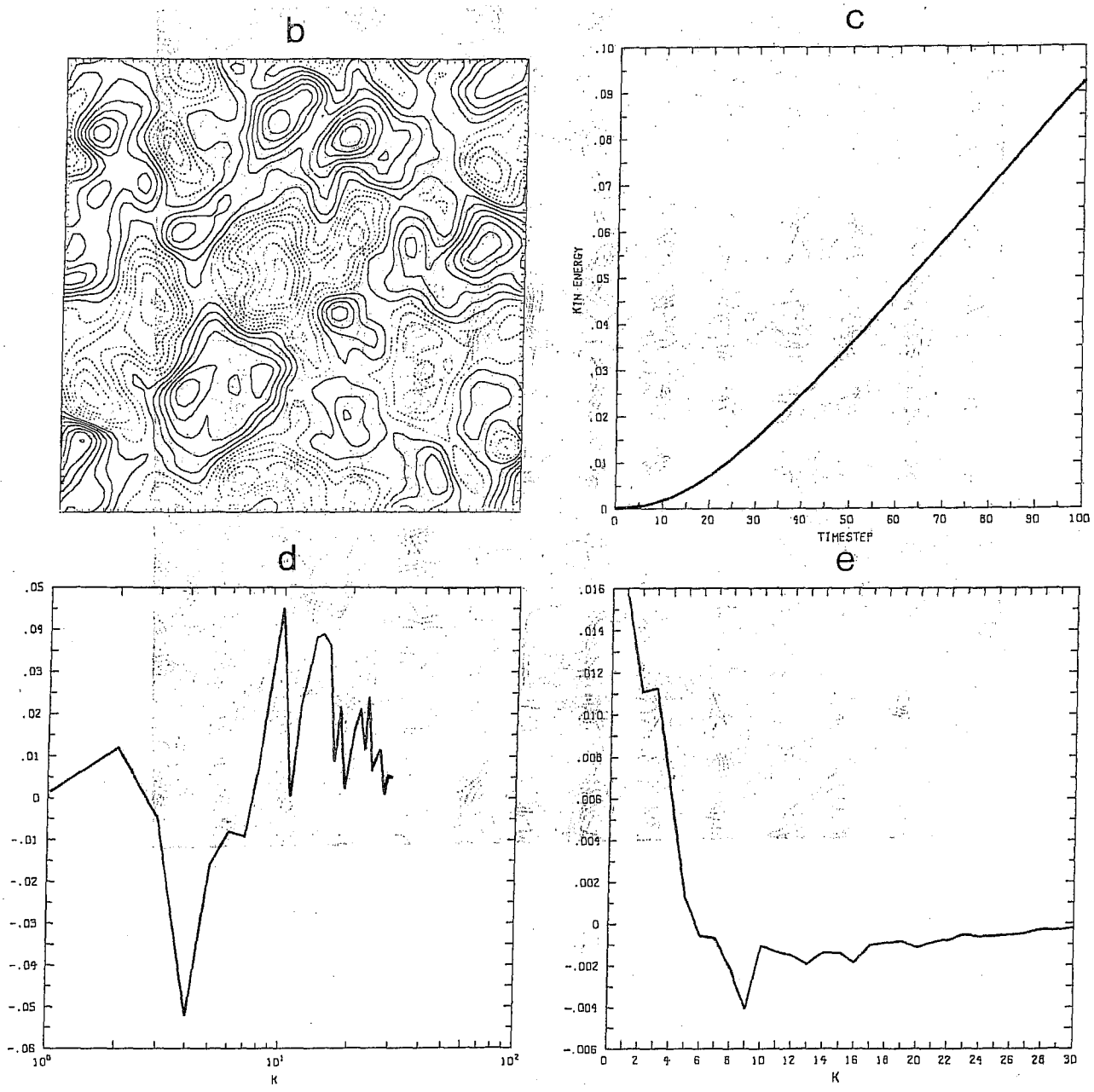

Fig. 4

THIS PAGE IS BLANK

Fig. 5. This example shows the evolution of the "frozen field" of log plankton as described in the text. Fig. 5a is a picture of the stream function field at t = 0, when the log plankton field, Fig. 5b, begins to be injected. Figures 5c and 5d show the net plankton field at two later times t = 2, and t = 4. Note the definite appearance of "patchiness" in the fields. Fig. 5e is a diagnostic of the plankton field and is Real (J^*Q) which indicates that scalar quantity is being advected out of wave numbers 2 through 4 (which are the injected wave numbers), and carried to higher wave numbers. This is intuitively correct.

a

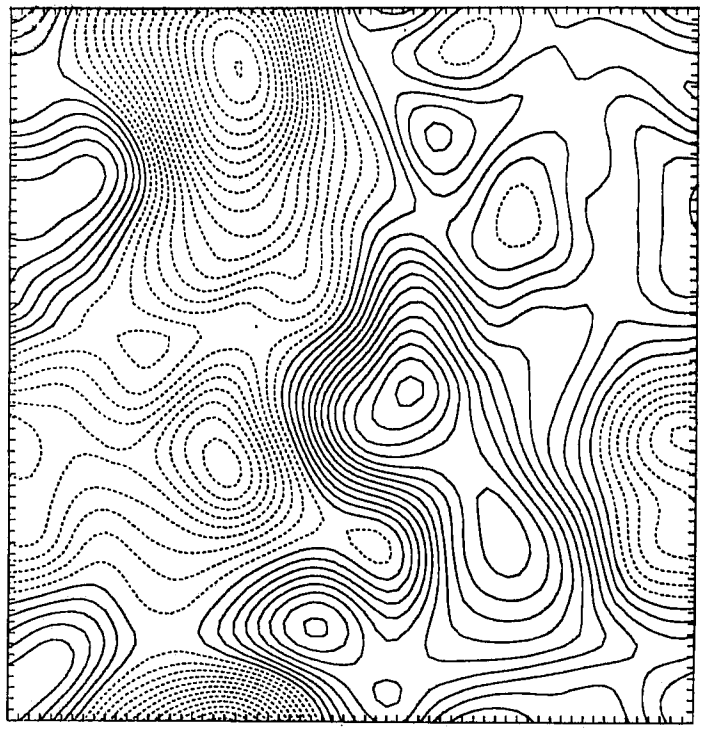

b

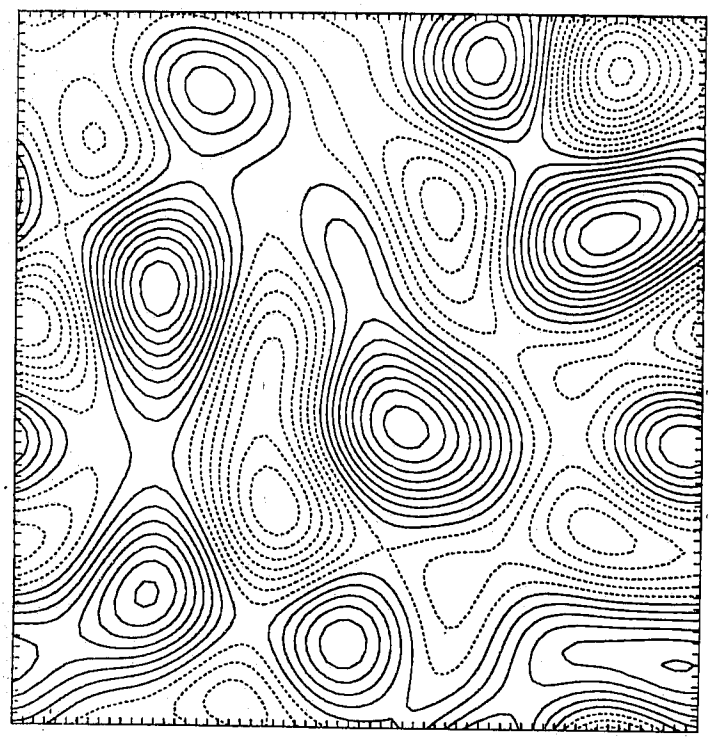

Fig. 5

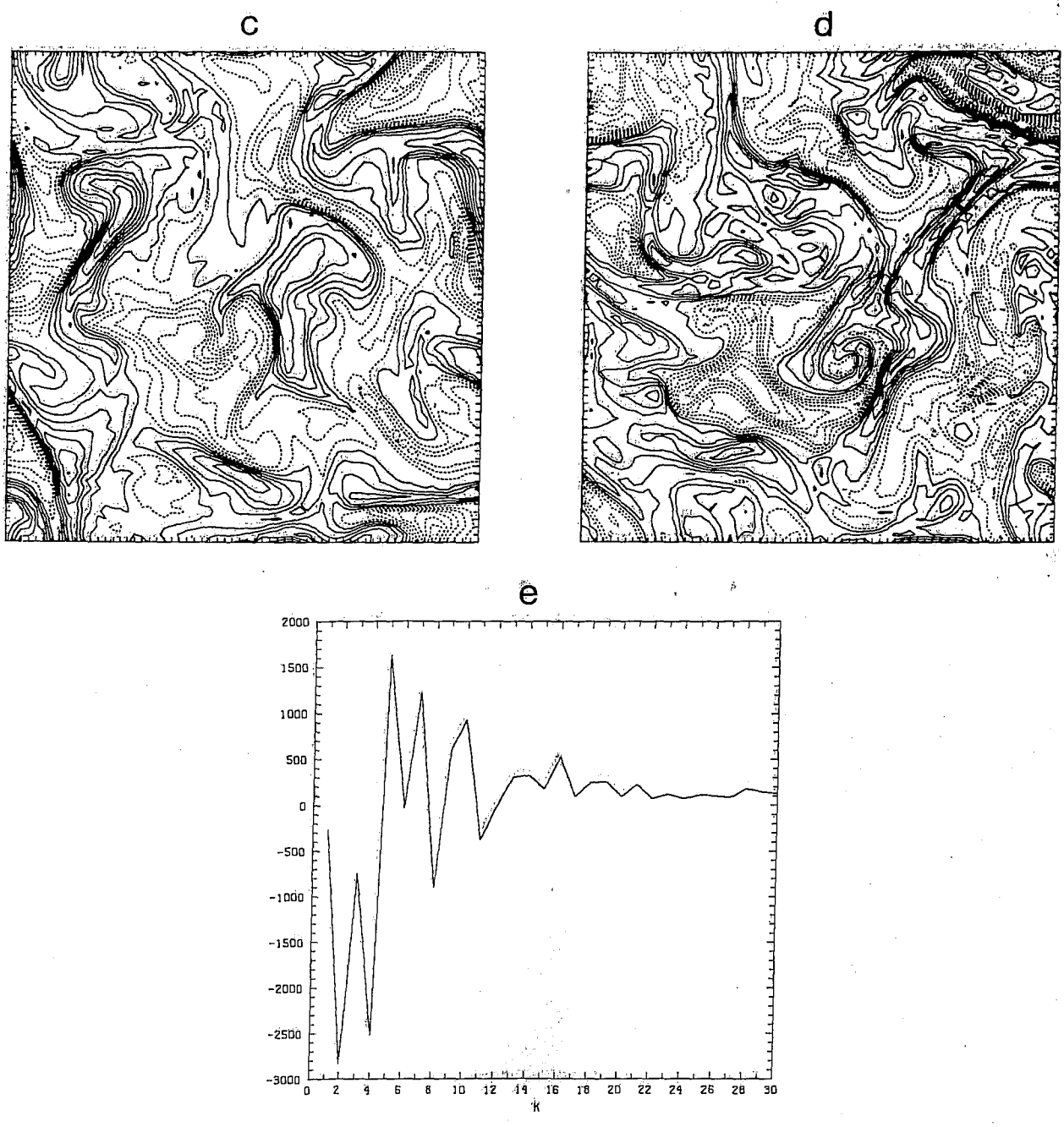
c
d
e
2000
1500
1000
500
0
-500
-1000
-1500
-2000
-2500
-3000
0 2 4 6 8 10 12 14 16 18 20 22 24 26 28 30
k

Fig. 5

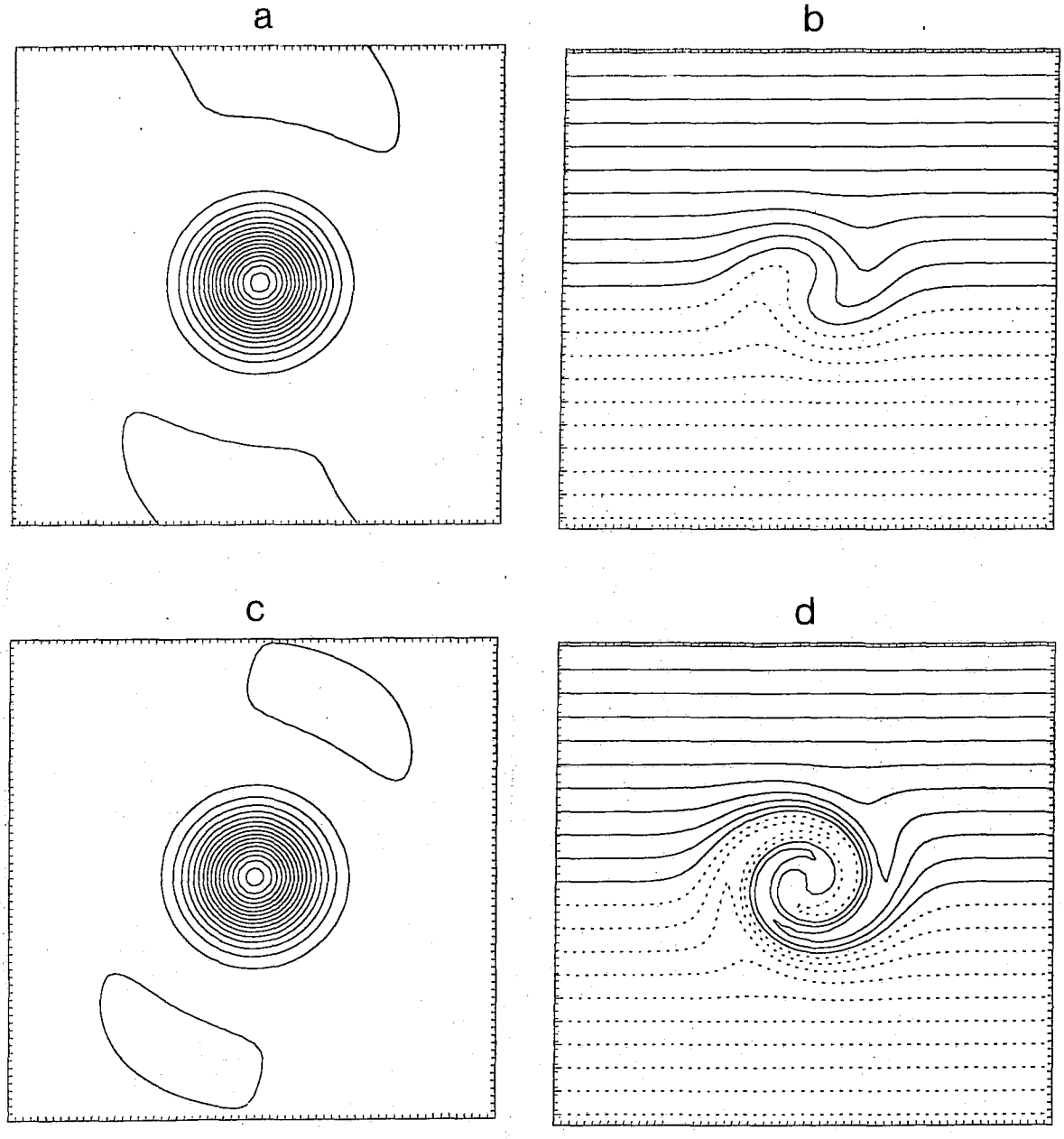

Fig. 6. This simple example shows that spectral methods do not distort physically realizable situations. In this example, a "spot" of turbulence evolves in figures 6a and 6c. A mean gradient of scalar quantity is added in the y direction, and figures 6b and 6d show how the turbulence spot "wraps up" the gradient quantity.

Fig. 7. This example shows the different effects of two types of the diffusion operator on an evolving Gaussian spot of scalar quantity. Fig. 7a evolves under the effect of $D\phi = \nabla^4\phi$. Fig. 7b evolves under exactly the same conditions as 7a except $D\phi = \nabla^2\phi$. Note the "fuzziness" of the ∇^2 operator since it operates on a wider range of wave numbers, whereas ∇^4 diffusion acts most strongly on only the highest wave numbers.

a

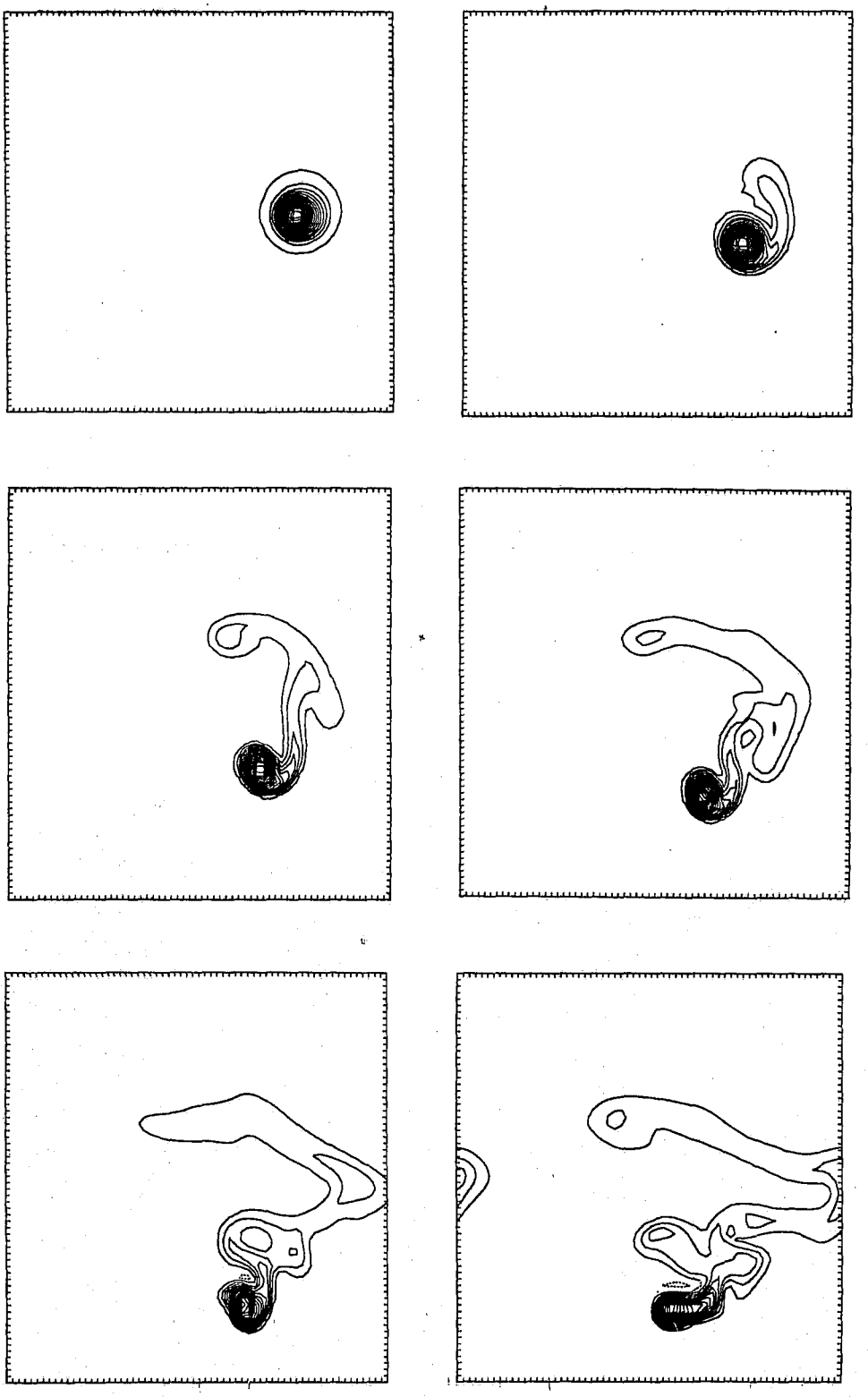

Fig. 7

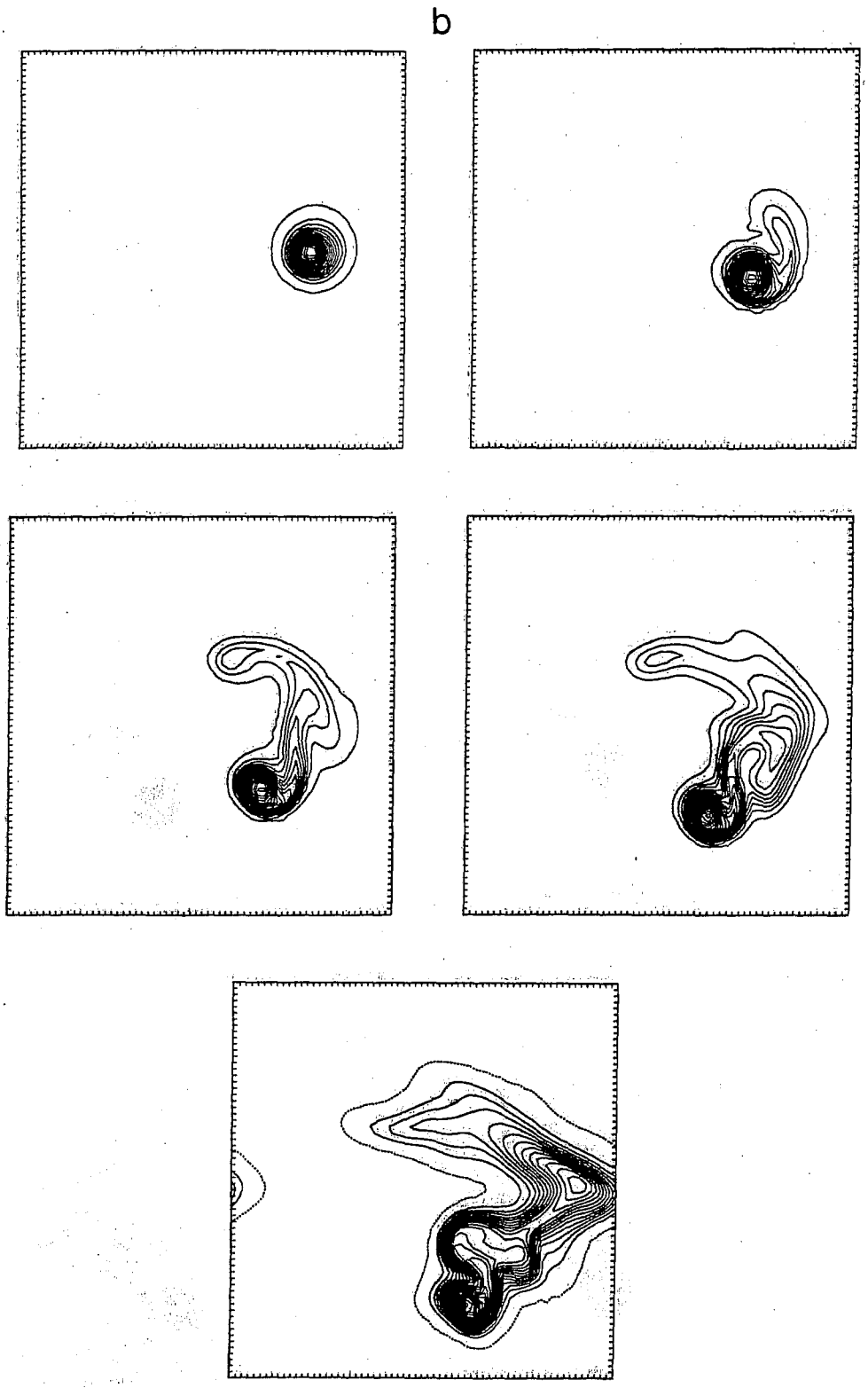

Fig. 7

THIS PAGE IS BLANK

Fig. 8. This example shows the Lagrangian particle capabilities of the methods and the effect of β on the floats. In Fig. 8a, 18 of 182 floats are shown released into a mature turbulence flow and allowed to evolve. Fig. 8b is exactly the same except for the presence of β. Note how β tends to stretch the motion out in the zonal direction. Figs. 8c and 8d show the average float pair separations in the x and y directions respectively for the case without β. Figs. 8e and 8f show the same for the case with β. Careful examination shows again how β emphasizes zonal separation, and suppresses meridional separation.

a

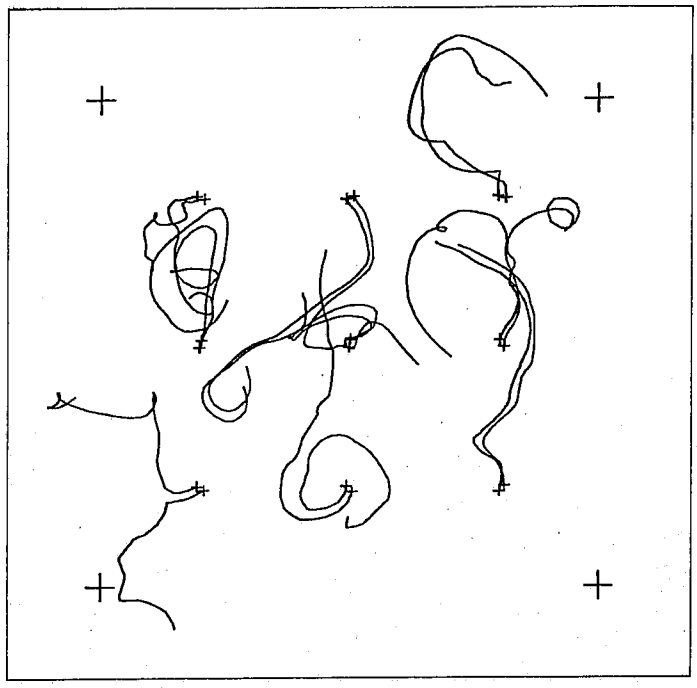

b

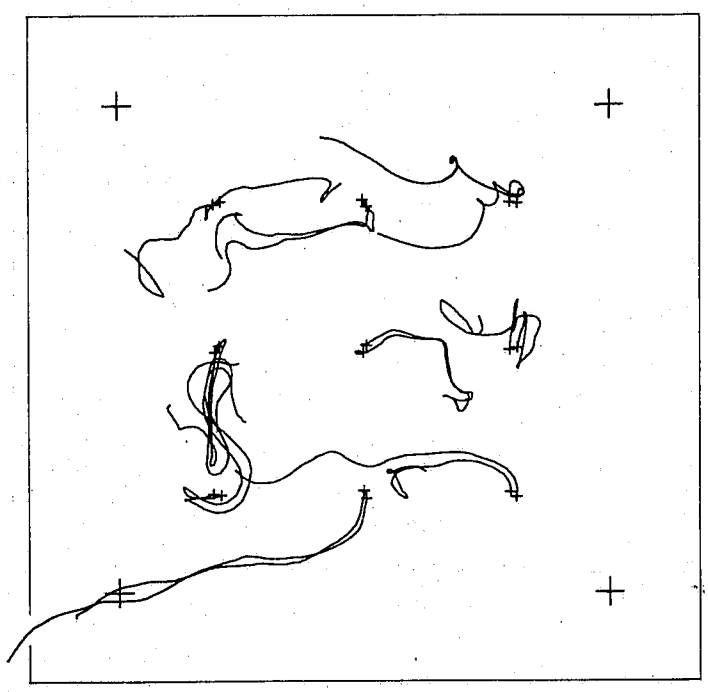

Fig. 8

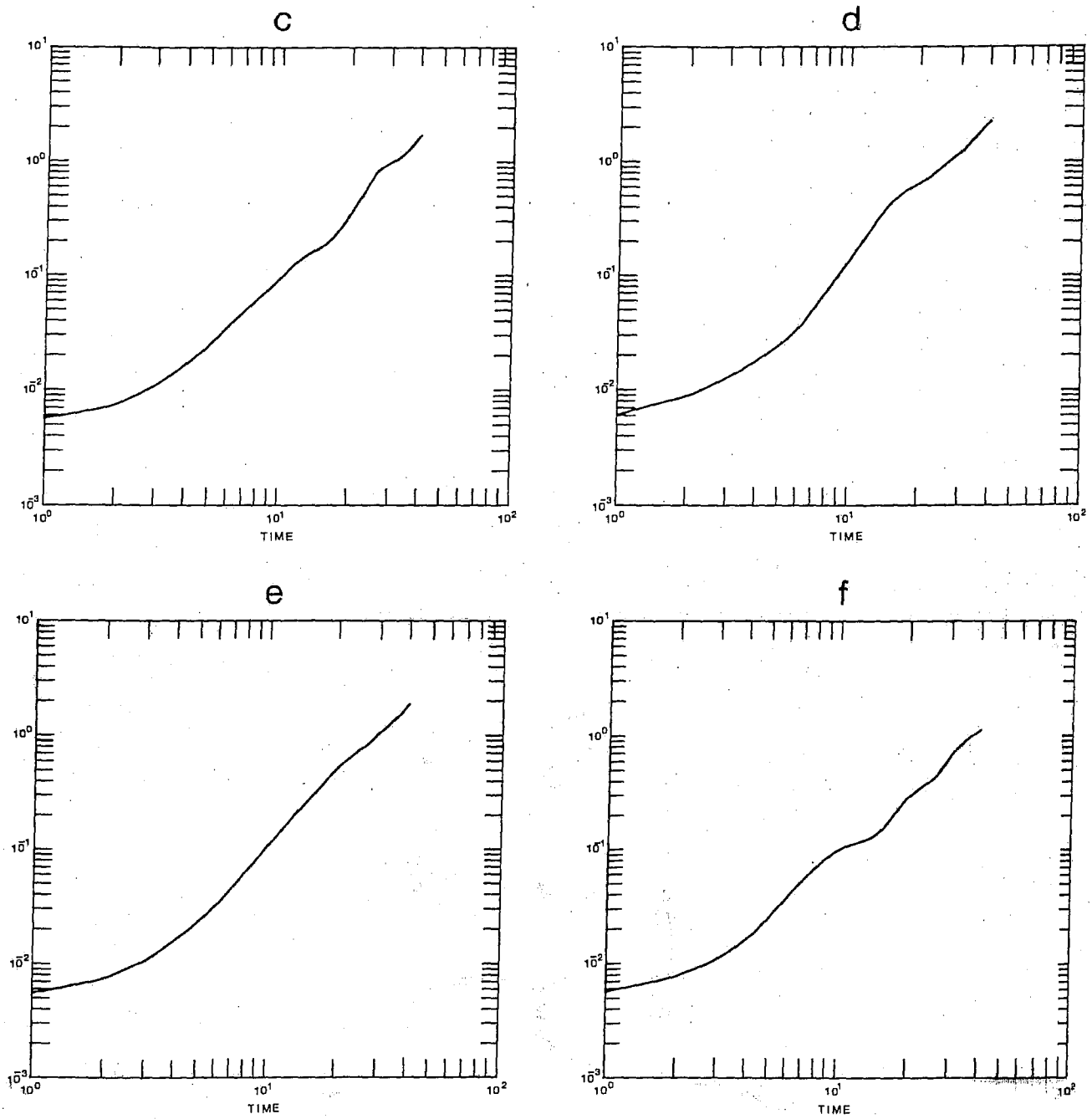

Fig. 8

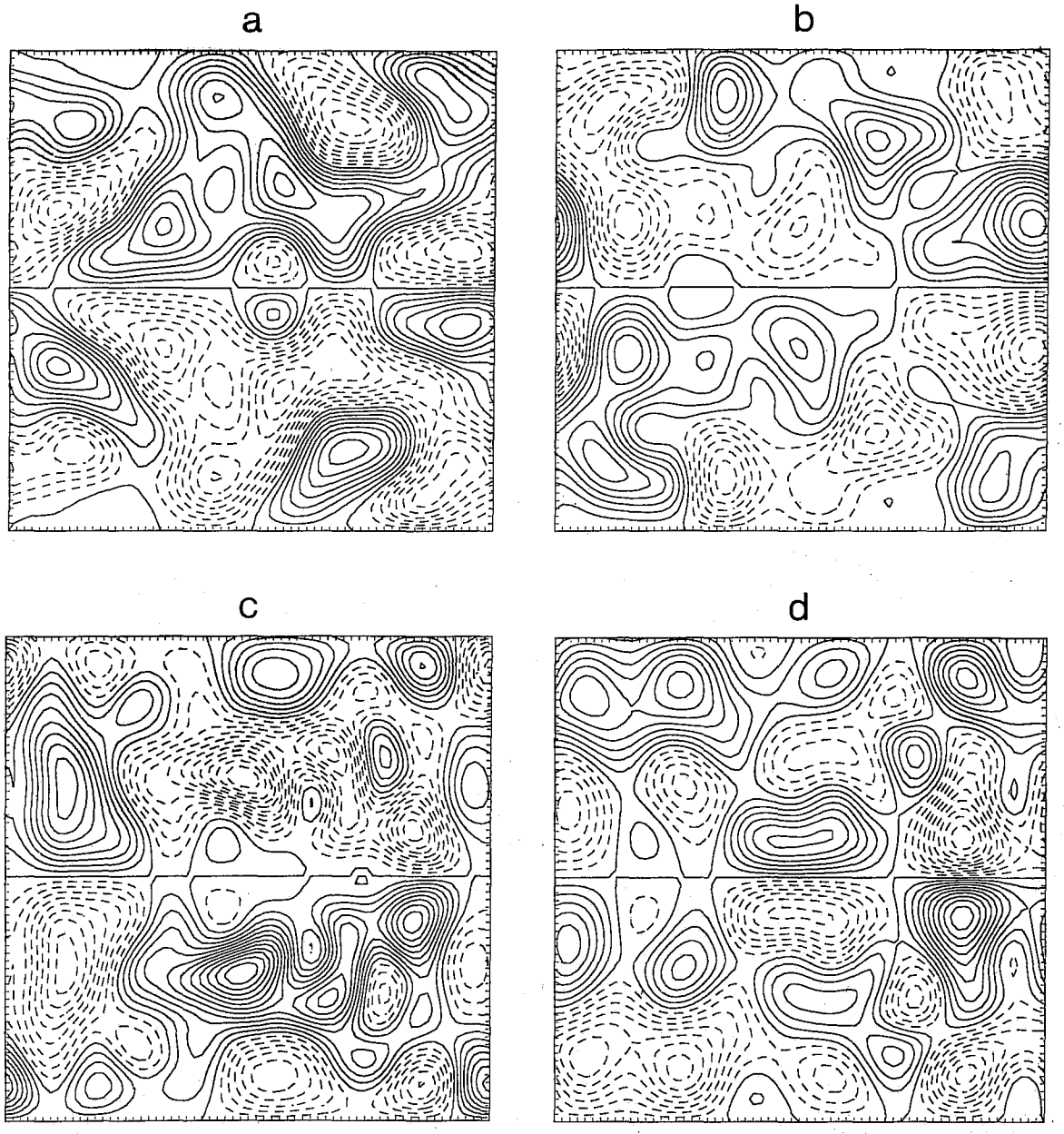

Fig. 9. This figure illustrates two current capabilities, layer flow contained between rigid walls in a free slip condition. In this example, no mean forcing was prescribed. The flow is baroclinically unstable due to the difference in mean flow between the two layers. Figs. 9a and 9c show the lower layer stream function at two times. Figs. 9b and 9d show the difference stream function at the same times. Note the redundancy in the plots. The top or bottom half of all plots could have been suppressed.

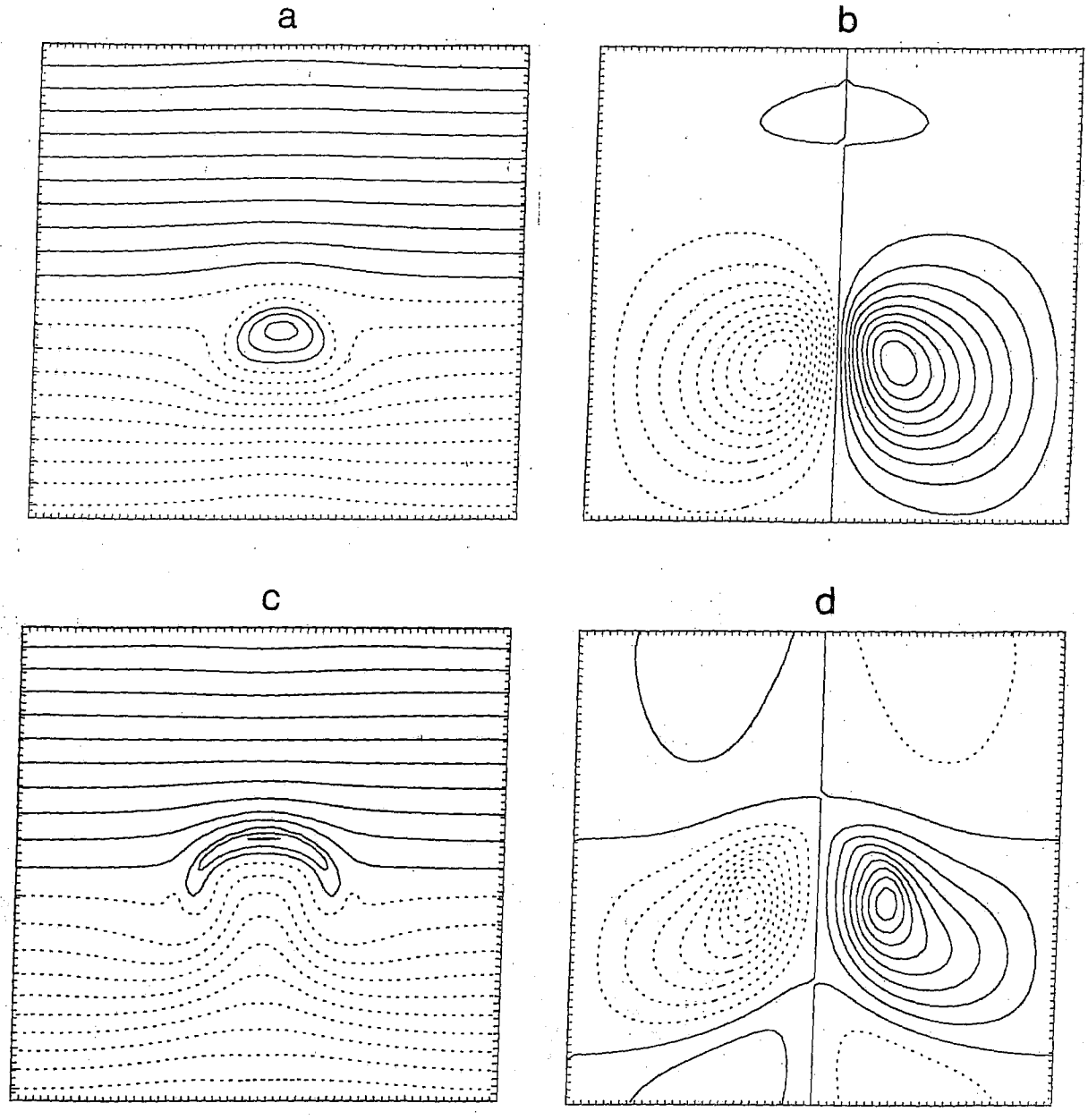

Fig. 10. This example shows the internal wave capability of the programs. A "spot" of buoyancy is placed into an initially quiescent water mass. Figs. 10a and 10c show the evolution of this spot at two later times against the background stabilizing buoyancy gradient. Figs. 10b and 10d show the resulting stream function field at the same times as 10a and 10c. Eventually, the "spot" will pass its equilibrium point and begin to move down again, hence, internal waves.